Received: 1 December 2023 | Revised: 20 February 2024 | Accepted: 26 February 2024
DOI: 10.1002/jbm.a.37703

RESEARCH ARTICLE

Impact of crystalline domains on long-term stability and mechanical performance of anisotropic silk fibroin sponges

Elizabeth L. Aikman[1] | **Asha P. Rao**[1] | **Yinhao Jia**[1] | **Emily E. Fussell**[2] | **Kayleigh E. Trumbull**[1] | **Janani Sampath**[1] | **Whitney L. Stoppel**[1,2]

[1]Department of Chemical Engineering, University of Florida, Gainesville, Florida, USA

[2]J. Crayton Pruitt Family Department of Biomedical Engineering, University of Florida, Gainesville, Florida, USA

Correspondence
Whitney L. Stoppel, J. Crayton Pruitt Family Department of Biomedical Engineering, University of Florida, 1030 Center Drive, PO Box 116005, Gainesville, FL 32611, USA.
Email: whitney.stoppel@ufl.edu

Present address
Kayleigh E. Trumbull, Department of Chemical and Biomolecular Engineering, Clemson University, Clemson, South Carolina, USA.

Funding information
National Science Foundation Graduate Research Fellowship, Grant/Award Number: DGE-2236414; National Science Foundation Research Experience, Grant/Award Number: EEC-1852111

Abstract

Sponge-like materials made from regenerated silk fibroin biopolymers are a tunable and advantageous platform for in vitro engineered tissue culture and in vivo tissue regeneration. Anisotropic, three-dimensional (3D) silk fibroin sponge-like scaffolds can mimic the architecture of contractile muscle. Herein, we use silk fibroin solution isolated from the cocoons of *Bombyx mori* silkworms to form aligned sponges via directional ice templating in a custom mold with a slurry of dry ice and ethanol. Hydrated tensile mechanical properties of these aligned sponges were evaluated as a function of silk polymer concentration (3% or 5%), freezing time (50% or 100% ethanol), and post-lyophilization method for inducing crystallinity (autoclaving, water annealing). Hydrated static tensile tests were used to determine Young's modulus and ultimate tensile strength across sponge formulations at two strain rates to evaluate rate dependence in the calculated parameters. Results aligned with previous reports in the literature for isotropic silk fibroin sponge-like scaffolds, where the method by which beta-sheets were formed and level of beta-sheet content (crystallinity) had the greatest impact on static parameters, while polymer concentration and freezing rate did not significantly impact static mechanical properties. We estimated the crystalline organization using molecular dynamics simulations to show that larger crystalline regions may be responsible for strength at low strain amplitudes and brittleness at high strain amplitudes in the autoclaved sponges. Within the parameters evaluated, extensional Young's modulus is tunable in the range of 600–2800 kPa. Dynamic tensile testing revealed the linear viscoelastic region to be between 0% and 10% strain amplitude and 0.2–2 Hz frequencies. Long-term stability was evaluated by hysteresis and fatigue tests. Fatigue tests showed minimal change in the storage and loss modulus of 5% silk fibroin sponges for more than 6000 min of continuous mechanical stimulation in the linear regime at 10% strain amplitude and 1 Hz frequency. Furthermore, we confirmed that these mechanical properties hold when decellularized extracellular matrix is added to the sponges and when the mechanical property assessments were performed in cell culture media. We also used nano-computed tomography (nano-CT) and simulations to explore pore interconnectivity and tortuosity. Overall, these results highlight the potential of anisotropic, sponge-like silk fibroin scaffolds for long-term (>6 weeks) contractile muscle culture with an in vitro bioreactor system that provides routine mechanical stimulation.

KEYWORDS
crystalline biopolymers, hysteresis, silk fibroin, tensile strength, viscoelasticity

1 | INTRODUCTION

Silk fibroin-based sponges have applications across tissue engineering and regenerative medicine. These sponges have been shown to be advantageous due to their tunable initial mechanical properties and ability to maintain their structure while also providing adequate microenvironments for cell growth, differentiation, or maturation.[1–7] Previous work has demonstrated the tunability of silk sponge-like biomaterials through modulation of polymer molecular weight, polymer concentration, pore structure and diameter, and induced crystallinity within the silk fibroin protein.[3,5,8] These tunable factors allow for modulation of the initial internal structure and mechanical properties of the sponges. Additionally, biomolecules can be included before or after the sponge formation to provide biologically relevant factors for different cellularized applications.[7] These materials also degrade over relevant time scales in vivo, with degradation rates that are tied to local enzymatic activity.[5,7,8] In vivo, the composition of the scaffold has a strong impact on cell infiltration and rate of material degradation.[1,7] Thus, biomaterials formed as silk or silk-composite sponges have shown promise for tissue engineering and regenerative medicine.[9]

Investigators have used silk materials as long-term (>6 weeks) in vitro culture platforms. Silk fibroin sponges have been shown to support long-term function of encapsulated or seeded cells for over 6 weeks, including cell types such as hepatocytes, fibroblasts, and adipocytes.[2,10,11] One advantage of these materials as long-term culture platforms is their ability to hold their size, shape, and volume as cells are introduced. In addition, seeded or encapsulated cells fill pore space or voids within the material as they grow and hypertrophy, rather than contracting the matrix and excluding water to reduce the volume and increase cell density, as seen in hydrogels.[12,13] Maintaining the structure and viability of muscle cells while also providing consistent mechanical stimulation over long time periods will enable future studies of muscle disease progression, atrophy, and mechanotransductive pathways for both fundamental and treatment-oriented studies, such as drug delivery. Furthermore, fundamental studies on mechanotransductive pathways, such as those that go awry in rare muscular dystrophies,[14] may shed light on disease mechanisms or disease progression. To date, these anisotropic silk fibroin sponge-like materials have been used for short-term studies of muscle progenitor cells or myoblasts,[1,3] suggesting the potential to support cell growth and maturation. The ability to induce anisotropy within these materials[1,3] makes them an ideal candidate for a long-term culture platform for contractile muscle.[1,15]

Ice templating, or freeze-casting, is a technique where ice crystals guide the generation of porosity within a material, as water phase separates from the polymer during the freezing process.[16–18] This technique can be useful in materials fabrication where porosity is an important fabrication parameter for mass transfer and cellular organization within a material. Tunable parameters such as freezing time, freezing temperature, and solution composition are among many factors that control porosity and internal structure.[16–18] Unidirectional ice templating enables fabrication of highly aligned materials through driving a freezing front in one direction across the polymer solution. This is commonly used for skeletal muscle applications,[17] and has been successful in generating aligned silk fibroin scaffolds for muscle applications.[1,3] In this work we utilize sponge-like biomaterial structures by unidirectionally freezing silk fibroin solution, freeze drying the structure, and then inducing crystallinity to produce a water insoluble scaffold, hereinafter referred to as sponges. We build upon previous work generating silk fibroin-based sponges[1,3,5,19–22] and focus on the mechanical structure–function relationships of these anisotropic sponges. In our work, fabrication parameters such as silk fibroin concentration, freezing rate, and crystallinity all play a role in the tunability of the dynamic responses of our aligned sponges, such as rates of degradation, internal structure, and other physical properties of the sponges, including mechanical properties.[7]

The driver of these anisotropic structures is the molecular organization of the silk fibroin proteins as water is excluded during the fabrication process.[23,24] As water is removed from the backbone, silk fibroin biopolymers form intra- and inter-molecular interactions in the form of hydrogen bonding to form beta-sheets. The overall protein has amorphous regions in addition to long regions of glycine–alanine–glycine–alanine–glycine–serine (GAGAGS) sequences that form the beta-sheets and subsequent crystalline regions. It is accepted in the *Bombyx mori* silk fibroin field that these beta-sheets are responsible for the resulting mechanical properties[23–25] and hypothesized that their organization can drive observed mechanics. In this work, we build on existing molecular dynamics (MD) simulations[26] of crystal structures to include computational analysis of stress–strain curves. We compare phenomenological results with observed rheological measurements to give insight into how crystal structure organization drives measurable mechanical properties, especially at high strain amplitudes.

For the translation of these anisotropic materials as a long-term culture platform for evaluation of muscle differentiation, maturation, and function, we must also gain a greater understanding of material performance over long time scales and continued mechanical stretch.

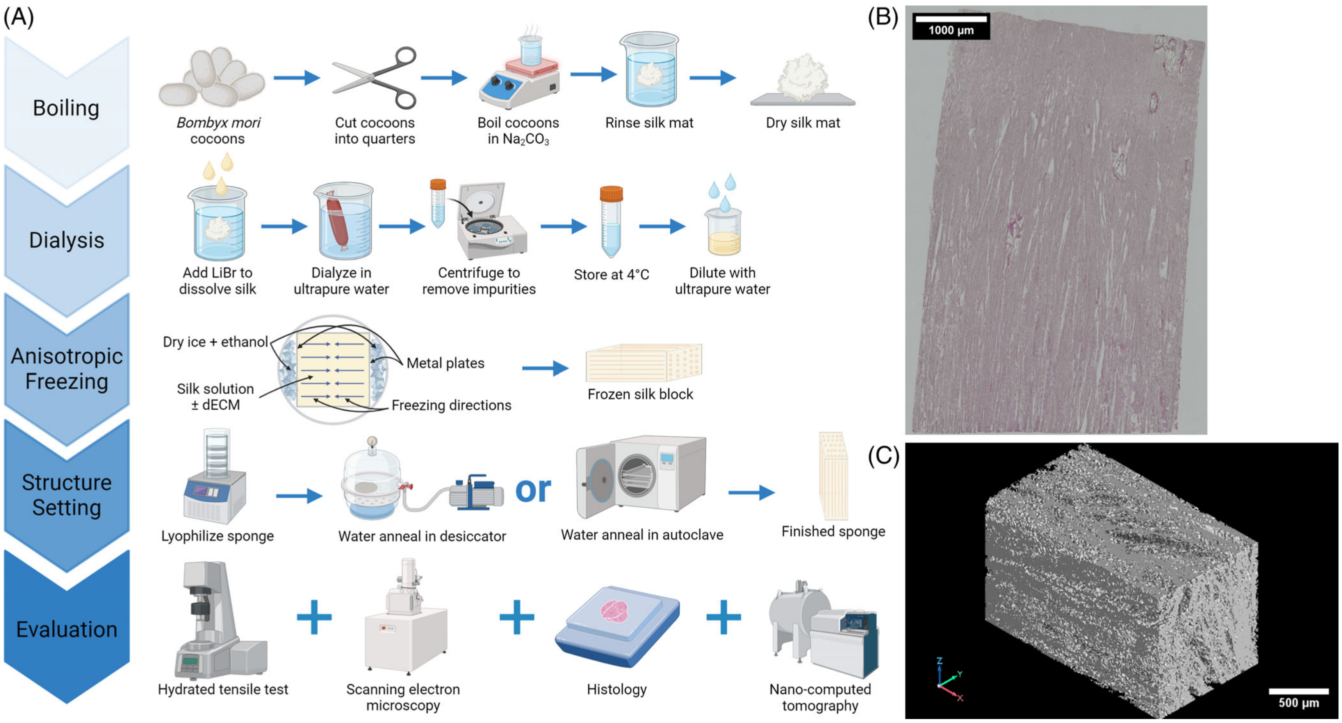

FIGURE 1 (A) *Bombyx mori* cocoons are boiled for 30 min and processed into aqueous silk fibroin solution. Silk fibroin sponges are made via directional freezing of the silk fibroin biopolymer solution in a custom mold. Following lyophilization and crystallinity induction, sponges are cut to appropriate sizes for imaging and mechanical testing. The accompanying Video S1 depicts how these dynamic mechanical analysis experiments are run. *Created with BioRender.com* (B) representative hematoxylin and eosin section to demonstrate alignment of anisotropic silk fibroin sponges from a top-down view (C) representative nano-computed tomography rendering of an anisotropic silk fibroin sponge. dECM, decellularized extracellular matrix.

Because of the complexity of biomaterials platforms necessary to mimic native tissue,[27] future work should emphasize the properties needed to ask a given hypothesis within a three-dimensional (3D) musculoskeletal platform. Key design parameters for many applications will include the initial static mechanical properties as well as dynamic mechanical properties. Understanding how these viscoelastic silk fibroin sponges behave over time is necessary for a fundamental understanding of force applied during mechanical perturbation in a bioreactor system. Initial mechanical properties of anisotropic silk scaffolds have previously been characterized through static compression testing over short time periods,[1] but hydrated tensile testing has not been utilized. Tensile testing, or the impact of continuous or repeated uniaxial stretch, is critical for understanding viscoelastic and elastomeric behavior during mechanical perturbation in a bioreactor.[15]

In this work, we explore the parameter space available for the generation of aligned 3D silk fibroin-based sponges, such as silk fibroin polymer concentration, freezing time, and post-lyophilization method to induce beta-sheet crystallinity. We identify the formulation parameters that drive structural properties, static mechanical properties such as extensional Young's modulus, and the dynamic viscoelastic behavior of these materials under cyclic strain. We hypothesize that the internal structure of the aligned silk fibroin sponges will drive the changes in mechanical properties of the system. Figure 1 summarizes the fabrication of these aligned silk sponges, revealing the resulting structural anisotropy through and hematoxylin and eosin (H&E) staining and nano-computed tomography (nano-CT). Figure 1 and Video S1 illustrate the experimental setup for hydrated, tensile testing using a custom cup for the linear drive of an Anton Paar MCR 702e rheometer system with dynamic mechanical analyzer clamps. We use this system to establish the initial anisotropic lyophilized silk fibroin sponge fabrication parameters (Table 1) that maintain their viscoelastic properties for >100 cycles without deformation, to identify initial formulations that may support culture of contractile muscle cells under dynamic cyclic strain to enable use as a long-term culture platform for applications in pharmaceutical studies, evaluation of disease mechanisms, or investigation of disease progression in contractile tissues.

2 | MATERIALS AND METHODS

2.1 | Silk fibroin extraction

Bombyx mori silk cocoons were cut and debris was removed.[28] Five grams of the cocoons were boiled in 2 L of sodium carbonate solution (0.02 M) for 30 min (Sigma-Aldrich, St. Louis, MO, USA) to remove sericin proteins coating the fibroin polymers.[1] After boiling, the degummed fibers were rinsed three times in ultrapure water for

TABLE 1 Fabrication parameters used to explore the influence of polymer concentration, pore structure, and crystallinity on the mechanical properties of anisotropic silk sponges.

Silk fibroin polymer concentration (wt/vol)	Freezing slurry (vol/vol) to impact porosity	Method to induce crystallinity	Symbol
3% Silk fibroin	50% Ethanol	6-h water annealing	🟠
3% Silk fibroin	100% Ethanol	6-h water annealing	🔵
3% Silk fibroin	100% Ethanol	Autoclaving	🔴
5% Silk fibroin	50% Ethanol	6-h water annealing	🟧
5% Silk fibroin	100% Ethanol	6-h water annealing	🟦
5% Silk fibroin	100% Ethanol	Autoclaving	🟥

Note: Colors and shapes used to denote the sample types throughout the manuscript are also provided.

20-min intervals.[28] After the rinses were completed, excess water was squeezed out and the silk mats were dried for 48 h. After drying, 9.3 M of aqueous lithium bromide (Sigma-Aldrich, St. Louis, MO, USA) was added to solubilize the pure silk fibroins.[1,28] Then, the silk fibroin solution was dialyzed by using 3.5 kDa MW cut off dialysis tubing against ultrapure water (3500 MWCO, ThermoScientific, Rockford, IL, USA).[1] After dialysis, the silk fibroin solution was removed from the tubing and centrifuged three times at 4000 RPM for 20 min at 4°C to remove insoluble particulates.[1] The solutions were stored in 4°C.[28] To find the resulting concentration of silk fibroin solution, the weight by volume percentage was found by drying the solution overnight and comparing the dry and wet masses. The silk fibroin solution was diluted with water to the desired concentration (% wt/vol) to be formed into sponges.

2.2 | Decellularized extracellular matrix

Adult skeletal muscle tissue was decellularized similar to tissues reported by Stoppel et al.[1] Adult porcine skeletal muscle (antibiotic free pork chops) was obtained from the supermarket (Whole Foods). The tissue was cut into small pieces (∼10 mm by 10 mm by 10 mm). Tissue pieces were washed with phosphate buffered saline (PBS) (Fisher Bioreagents, Pittsburgh, PA, USA) containing 1% pen-strep for 30 min, then decellularized with 1% (wt/vol) sodium dodecyl sulfate (SDS) (Boston Bioproducts, Milford, MA, USA). The SDS solution was changed every 2 h on the first day and three times per day until the tissue appeared white and was completely decellularized. The extent of decellularization was confirmed through wax embedding, sectioning, and H&E staining to ensure all the cells have been removed. The decellularized pieces were then washed in ultrapure water for 48 h to remove the SDS. The pieces underwent acetone precipitation to remove any unwanted small molecules or residual SDS, then rinsed three times in ultrapure water for 20 min each. The decellularized tissue was then frozen at −80°C for 24 h and lyophilized (Labconco, Kansas City, MO, USA) for 48 h. The pieces were milled through a 40 mm mesh on a single speed mini cutting mill (Thomas Scientific, Thorofare, NJ, USA) and then solubilized through pepsin digestion in 0.1 N HCl (LabChem, Zelienople, PA, USA). After digestion, pepsin was neutralized with 1 M sodium hydroxide (Fisher Chemical, Pittsburgh, PA, USA). The decellularized extracellular matrix (dECM) solution was frozen and lyophilized until use, where it was diluted with ultrapure water to a concentration of 5 mg dECM/mL water. Then, this stock solution is used to create silk fibroin solutions with dECM at a concentration of 0.2 mg/mL of total volume. The ratio of silk fibroin to pepsin-digested, reconstituted dECM is either 30 (3% wt/vol) to 0.02 mg/mL or 50 (5% wt/vol) to 0.02 mg/mL. These ratios and concentrations were chosen based on previous evaluation of these materials, which showed this 1500–2500 fold difference in silk fibroin to dECM concentration meant that the silk fibroin dominated the resulting previously measured material properties.[1]

2.3 | Sponge formation

In this study, the fabrication parameters of the sponges were polymer concentration (3% and 5% silk fibroin), freezing rate (50% and 100% ethanol), and crystallinity (water annealing for 6 h and autoclaving). The concentration of sponges was set based on previously stated procedures. For the formulations requiring dECM, 0.2 mg/mL of dECM was gently mixed with the diluted silk fibroin solution prior to freezing.[1] In addition, to mimic skeletal muscle tissue alignment, the sponges were frozen in an anisotropic or aligned direction previously described by Stoppel et al.[1] The freezing arrangement occurred by placing a dry ice and ethanol (50% or 100% [vol/vol] ethanol) slurry on one side of a metal divider and the silk solution on the other. 184 Sylgard elastomer (Dow Corning, Midland, MI, USA) was used as the base to help maintain the metal mold.[1] The silk solution froze across the container starting at the metal plate and moving across the solution. The water in the solution freezing first caused phase separation of the water and silk. The resulting frozen silk and water block was put on a lyophilizer (Labconco, Kansas City, MO, USA) to sublimate the ice and remove it from the sample. This lyophilization produced a water soluble silk sponge, due to the pores that were created when the ice crystals were sublimated. The post-lyophilization methods produced different crystallization levels by autoclaving (120°C and 0.101 MPa) or 6-h water annealing (23°C and 0.023 MPa) and renders the final sponge water insoluble. From the large sponge sample, smaller strips were cut out for imaging or mechanical testing.

2.4 | Scanning electron microscopy

Cross sectional pieces of the hydrated 3D sponges were cut to examine the *x*, *y*, and *z* planes of the sponge. Samples were attached to conductive tape mounted on ZEISS/LEO SEM Pin Stub Mount, Ø12.7 mm × 9 mm pin height (Catalog No. 16202, Ted Pella, Inc., Redding, CA) and left to dry in a fume hood for 48 h. The samples were imaged via a Phenom Pure benchtop SEM (ThermoFisher Scientific, Waltham, MA, USA) in a charge reduction sample holder at 5 kV and 500× magnification to confirm alignment and architecture structure (Figure S1). ImageJ (US NIH, Bethesda, MA, USA) was utilized for analysis of the SEM images.

2.5 | Fourier transform infrared spectroscopy

Fourier transform infrared spectroscopy (FTIR) was used to gain insight into the secondary structure and crystalline content of the different post-lyophilization methods (water annealing or autoclaving). The sponges were analyzed using attenuated total reflection with a germanium crystal on a Nicolet iS50 FTIR Spectrometer (ThermoFisher Scientific, Waltham, MA, USA). Each sample was analyzed for a total of 4 technical replicates ($n = 4$) with spectra gathered over 128 scans at a resolution of 4 cm^{-1}. Representative spectra before deconvolution can be found in Figure S2 to demonstrate the shift in peak location and amplitudes. The wavenumber range collected spanned from 4000650 cm^{-1} with the amide I region at 1590–1720 cm^{-1} of interest to the secondary structure of silk fibroin. The background spectra were collected at the same conditions to be subtracted from the sample spectra and then analyzed with OriginPro, Learning Edition Version 2023 (OriginLab Corporation, Northampton, MA, USA). The deconvolution of the secondary structure was performed according to Hu et al.[24,29] This deconvolution included: 1605–1615 cm^{-1} as side chain/aggregated strands, 1616–1637 cm^{-1} and 1697–1703 cm^{-1} as beta-sheet structure, 1638–1655 cm^{-1} as random coils, 1656–1662 cm^{-1} as α-helical bands, and 1663–1696 cm^{-1} as turns.

2.6 | Hydrated tensile mechanical analysis

Prior to mechanical testing, the silk fibroin sponges were hydrated in ultrapure water for 24 h. For more relevant analysis samples were also hydrated in cell culture medium containing fetal bovine serum (FBS) (Human Skeletal Muscle Growth Medium with Supplement Mix) (PromoCell, Heidelberg, Germany) or serum free growth medium, DMEM/F-12 with GlutaMAX supplement (Life Technologies, Carlsbad, CA) for 24 h prior to testing. The width and thickness of the sponge samples were measured with digital calipers (18 mm by 8 mm by 2 mm). The dynamic mechanical analyzer setup was used on an Anton Paar MCR 702e Rheometer (Anton Paar, Graz, Austria), as shown in Figure 1 and Video S1. Each sample was placed into tensile clamps, and the clamps were tightened to 10 cN m with a torsion screwdriver. The upper clamp of the MCR 702e was the U-SRF5 clamp, and the lower clamp was the L-SRF5/LD/clamp. The gap width was recorded as the height of the sample (∼12 mm) between the clamps. A custom immersion cup system (Anton Paar) was attached to the instrument to keep the samples hydrated in water (or medium) during testing. Anton Paar RheoCompass software was utilized to perform static and dynamic tensile testing. Each of the following tensile tests included a pre-stretch at 0.1 N to ensure the sample did not sag.

2.6.1 | Static extension

Hydrated static testing was used to extend the samples from rest to 100% strain of their original length. Static tests were run at 1% per minute or 10% per minute strain amplitudes. Six samples for each sponge formulation were used ($n = 6$). From each static test, the Young's modulus and ultimate tensile strength (UTS) were calculated from the stress–strain curves. Analysis of the Young's modulus can be found in Figure S3. The mean ± standard deviation for the Young's modulus and UTS values hydrated in water can be found in Table S2.

2.6.2 | Amplitude sweep

In the amplitude sweep, the distance of the sample was extended linearly between data points, with a range of 0% strain–100% strain or complete failure, whereas maintaining the frequency value at 1 Hz. The testing was completed on six samples per formulation ($n = 6$). Most samples fractured completely around 60% strain amplitude. Representative amplitude sweeps for each sample formulation can be found in Figure S4.

2.6.3 | Frequency sweep

In the frequency sweeps, the amplitude was held constant at 10% strain and the frequency of these perturbations increased linearly from 0.2 to 10 Hz. The custom-made immersion cup did not allow for frequency readings beyond 10 Hz as the water would begin to spill, suggesting that air and fluid flow within the system may disrupt measured values. The testing was done on six samples per formulation. Representative frequency sweeps for each sample formulation can be found in Figure S5.

2.6.4 | Hysteresis tests

Hysteresis trials occurred at 10%/min from 0% to 10% strain amplitudes over 100 cycles. We confirmed the linear range agreement in Figure S6 with the static extensional tests previously performed. Five percentage silk fibroin sponges made with 100% ethanol freezing solution and either autoclaving or water annealing were used for hysteresis testing due to the crystalline content having the biggest impact on static mechanical properties and oscillatory sweeps.

2.6.5 | Fatigue tests

Fatigue tests were run at 1 Hz and 10% strain amplitude over the course of 6000 min. The samples chosen for the tests were the same types of sponges used for hysteresis trials to demonstrate the long-term response at different levels of beta-sheet crystalline content.

2.7 | Histological staining

The sponges were gently rinsed with PBS then cut to the desired size and geometrical arrangement before being fixed in 10% phosphate buffered formalin (Fisher Scientific, Hampton, NH, USA) and left to fix overnight at 4°C. Next, the sponges were dehydrated through a series of increasing ethanol concentration solutions. The sponges were cleared with xylene (Fisher Scientific, Hampton, NH, USA) so that the samples could be embedded in paraffin wax. The wax-embedded samples were mounted in wax cassettes in the desired orientation for sectioning, then sliced into 10 μm thick sections with a microtome (Microm HM355S), mounted on glass slides, and dried overnight on a slide warmer. The sections were deparaffinized and rehydrated with xylene followed by a series of decreasing ethanol concentrations before being stained with H&E. Finally, the slides were dehydrated again, and cover slips were mounted on the stained sections for imaging on a microscope (Keyence BZ-X800, Osaka, Japan).

2.8 | Molecular dynamics

Two silk fibroin chains comprised of both amorphous and crystalline regions, were constructed. The crystal region was modeled using the theoretical beta-sheet structure of silk fibroin (pdb: 1SLK)[30] and was further processed using VMD[31] and GROMACS[32] to generate a continuous beta-sheet chain. The sequence of the amorphous region was obtained from the *Bombyx mori* silk fibroin heavy chain. The model silk fibroin chain was built by linking the amorphous and crystal regions in two ways to give two different structured systems. Chain A consisted of two long continuous crystal regions and Chain B consisted of six discrete crystal regions. In both systems, the crystalline domains are connected by amorphous chains. The total molecular weight of the crystalline and amorphous domains in both systems is approximately 59 and 57.5 kDa, respectively. Each simulation box consists of four chains stacked to form a 2 × 2 matrix (Figure S7). The resulting systems have a total molecular weight of 236 (Chain A) and 230 kDa (Chain B).

2.8.1 | Tensile testing of modeled silk fibroin chains

Uniaxial deformation of the two systems was performed using the LAMMPS[33] package. CHARMM36m[34] forcefield was used to parameterize the protein, which is not solvated. The topology of the simulated systems was generated using the GROMACS *pdb2gmx* tool. The obtained topology was further processed using ParmED[35] and converted into LAMMPS style topology using the *ch2lmp* tool available in LAMMPS. The force-switching function was used to represent the van der Waals interactions. The cutoff for short-range electrostatic and van der Waals interactions was set with an inner and outer cutoff of 8 and 12 Å, respectively. Nose-Hoover thermostat and barostat were used to maintain constant temperature and pressure. The temperature and pressure were set to 300 K and 1 atm with damping factors of 200 and 2000 fs, respectively. The time step for numerical integration was 2 fs. Initial velocities were randomly assigned according to the Gaussian distribution corresponding to a temperature of 300 K. The simulation systems were first equilibrated under the NPT ensemble at 300 K and 1 atm for 2 ns, with bonds (including hydrogen bonds) constrained by the SHAKE[36] algorithm. The convergence of the system was evaluated by plotting the energy profile as well as the density along the simulation time. After equilibration, uniaxial deformation was applied using the deform function in LAMMPS. Specifically, tensile deformation was applied along the *z*-axis of the simulation box, which corresponds to the direction in which silk protein fibroin extends. The barostat was maintained in the *x* and *y* directions to regulate the overall pressure of 1 atm with a damping factor of 200 fs. The box was scaled at every timestep in the *z*-direction by applying a multiplicative factor, such that the final elongation length (strain) of the box was twice its original length. In this way, the strain rate was controlled by the number of steps needed to achieve the assigned factor. Here, the two constructed systems were deformed at strain rates of 25×10^9 sec^{-1}, 50×10^9 sec^{-1}, and 100×10^9 sec^{-1} (Video S2), corresponding to 40,000, 20,000, and 10,000 MD simulation steps, respectively.

2.9 | Nano-computed tomography

Assessment of the internal structure and porosity was conducted using nano-CT at the University of Florida Nanoscale Research Facility. Small sections of the 5% silk fibroin, 100% ethanol, and 6-h water annealed sponge (1.7 mm by 1.2 mm by 1.5 mm) and the 5% silk fibroin, 100% ethanol, and autoclaved sponge (2.6 mm by 1.5 mm by 1.5 mm) were stained with Lugol's solution (Sigma-Aldrich, St. Louis, MO, USA) for 24 h. The stained sponge pieces were rinsed with ultrapure water for 12 h on a rocking plate. The sponges were then imaged (Figure S8) via an Xradia 620 Versa (Carl Zeiss X-Ray Microscopy, Oberkochen, Baden-Württemberg, Germany) and analyzed using VGStudio Max (Volume Graphics GmbH, Heidelberg, Germany).

2.9.1 | Pore interconnectivity analysis via blender

The 3D reconstruction from nano-CT was converted to a mesh using VGStudio Max (Volume Graphics GmbH, Heidelberg, Germany). The meshes were imported into Blender v3.6 (Blender, Amsterdam, Netherlands) using the Bullet Physics engine add on and set to passive rigid body mesh collision settings. To assess pore interconnectivity, 50 sphere particles of a set diameter (5, 10, or 50 μm) and set mass of 1 kg, were dropped in the direction of alignment into the top of the mesh (Video S3). The spheres were simulated as active spherical collision shapes and were aligned in five rows of 10 spheres each evenly spaced over the top of the sponge before being dropped. The retention of the spheres was calculated from snapshots of the sphere particles in the sponges using ImageJ (US NIH, Bethesda, MA, USA).

2.10 | Statistical analysis

GraphPad Prism was used for statistical analysis. Analysis was performed with 1-way ANOVA with Tukey's test post hoc analysis. Statistical significance is reported as $^{*}p < .1$; $^{**}p < .05$; $^{***}p < .01$; $^{****}p < .001$. In the development of natural materials, there are a variety of situations that can lead to wide variability in our samples. The main cause of variability results from the natural source of the material as the *Bombyx mori* silkworm is commonly cultivated outdoors, where known changes in climate (temperature, humidity) may be impacting the silk production and viability of the silkworm. Although our batch-to-batch variability is relatively low, the spread in molecular weight leads to variability in polymer chain length within our polymer solutions.[37] Thus, reducing the stringency of the p value to include samples that are different with 90% confidence is worthwhile in the discussion of these samples.

3 | RESULTS AND DISCUSSION

To begin to assess the parameter space available for creation of anisotropic materials for applications in in vitro or in vivo use, we divided the potential driving factors for mechanical properties into three main groups which focus on total polymer concentration, porosity, and crystallinity from post-lyophilization method, as shown in Table 1. Thus, for different silk sponge formulations, we specifically evaluated the influence of polymer concentration (3% vs. 5%), freezing rate (50% vs. 100% ethanol), and crystallization level through post-lyophilization methods (autoclaving vs. water annealing). Silk fibroin concentrations were chosen based on easily obtainable concentrations during polymer extraction, which have been previously used to explore isotropic silk fibroin sponges.[5] Freezing rates were chosen based on total fabrication time for a slow and fast freezing time, where the 100% ethanol results in a freezing rate that is twice as fast as the 50% ethanol. The two post-lyophilization methods were chosen based on their applications. Water annealing in a vacuum desiccator or vacuum oven is a commonly used method to induce crystallinity and has been extensively used for silk fibroin materials.[1,4,5,8] Autoclaving is an alternative post-lyophilization method to induce beta-sheet formation, whereas also being a common technique for biomaterial sterilization before culture. Thus, the effects of these parameters will be evaluated as they are relevant to future applications of this anisotropic silk fibroin sponge.

Initially, six different types of sponges were generated following slight modifications to previously described methods to generate aligned silk sponges for these different parameters.[1] We qualitatively and quantitatively confirmed anisotropy of the sponges through scanning electron microscopy (SEM) analysis (see Figure S1). We expect to identify the role of porosity, pore anisotropy, and total crystalline content on static and dynamic mechanical properties, as SEM images show substantial differences in pore architecture. In our experimental design, we expected that changing the rate of freezing, by reducing the freezing slurry temperature through a reduction in ethanol, would cause the pore size to increase. The freezing rates with 50% ethanol solidified the silk fibroin solution at a rate of 0.44 mm per minute and the 100% ethanol freezing slurry produced 1.05 mm per minute rate of freezing through the silk fibroin solution. This freezing rate was not affected by the silk concentration, which had been previously confirmed for other freezing conditions.[3] This freezing mechanism can be seen in Figure 1 and the freezing rates for each silk fibroin and ethanol concentration combinations are reported in Table S1. We also expected that as we increased silk concentration from 3% to 5%, that we would see shifts in the thickness of the silk fibroin sheets that make up the pore walls. Differences in pore architecture were previously seen by Joukhdar et al.[3] and we confirm this architecture through modified fabrication methods and conditions. We performed tensile testing next to elucidate the effect that the fabrication parameters and pore architecture have on mechanical properties. This tensile testing was performed parallel to the direction of alignment, for biological relevance to muscle, on samples that had been hydrated for 24 h prior to testing and remained hydrated through the duration of the test.

3.1 | Static tensile mechanical property analysis

Representative SEM images in Figure 2 clearly show that concentration changes have a greater impact on observed pore diameter (vertical comparisons, Figure 2A vs. Figure 2C and Figure 2B vs. Figure 2D) than the reduction in freezing time (horizonal comparisons, Figure 2A vs. Figure 2B and Figure 2C vs. Figure 2D). These results are surprising, as we expected that the temperature of the freezing slurry, which controls the freezing rate, would have a greater impact based on previous results evaluating isotropic sponges formed at -20 versus -80°C.[2] However, the stark observed differences between polymer concentrations suggests that polymer–polymer interactions may drive sponge architecture more at 5% compared with what had previously been observed at 3%. Lower concentrations of silk fibroin polymer solution produce sponges with more mesh-like structure and higher concentrations produce more lamellar architecture with distinct wall and pore shapes.[2,5,22] These porosity assessments of anisotropic sponges are confirmed by previous work with various silk fibroin concentrations and a similar freezing apparatus.[3] We looked to understand the mechanisms by which these fabrication parameters affect mechanical properties of the sponges. We demonstrated that the sponges extended parallel to the direction of alignment are most

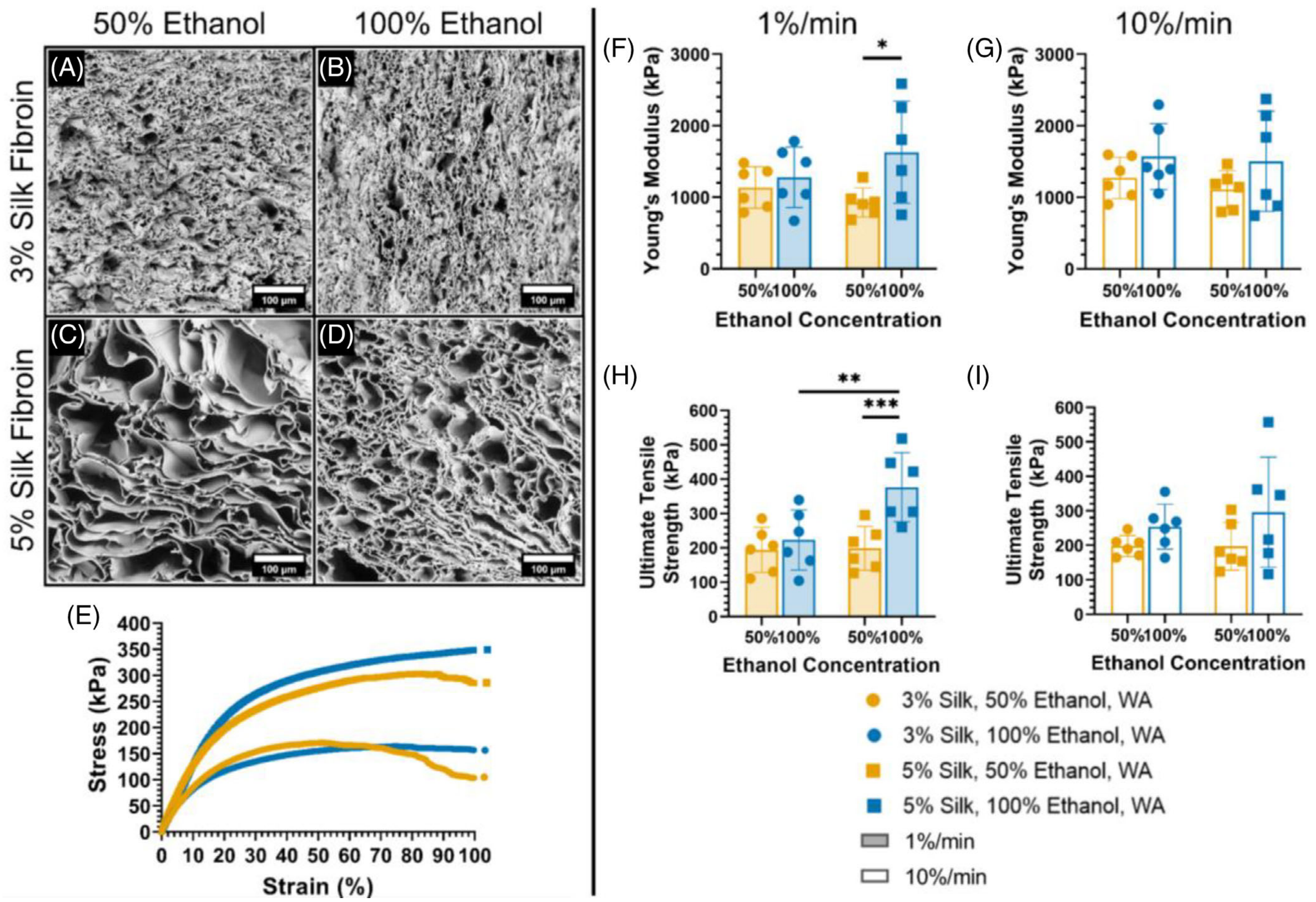

FIGURE 2 Structural images and static mechanical properties of anisotropic silk fibroin sponges formed with different silk concentrations and freezing rates (A–D) scanning electron microscopy cross-sections into the direction of alignment of sponges formed with different fabrication parameters (A) 3% silk fibroin concentration, 50% ethanol freezing solution, and 6-h water annealing (B) 3% silk fibroin concentration, 100% ethanol freezing solution, and 6-h water annealing (C) 5% silk fibroin concentration, 50% ethanol freezing solution, and 6-h water annealing (D) 5% silk fibroin concentration, 100% ethanol freezing solution, and 6-h water annealing. (E) Representative stress–strain curves at a rate of 10% strain per minute. (F–G) Average Young's modulus values for different sponge fabrication parameters ($n = 6$) (F) 1% strain per minute (G) 10% strain per minute. (H–I) Average ultimate tensile strength values for different sponge fabrication parameters ($n = 6$) (H) 1% strain per minute (I) 10% strain per minute. Data are expressed as mean ± standard deviation. Analyzed with 1-way ANOVA with Tukey's test post hoc analysis. Statistical significance is reported as $^{*}p < .1$; $^{**}p < .05$; and $^{***}p < .01$.

relevant to applications in tissue engineering as compared to usage perpendicular to the direction of alignment (Figure S3d). If visible and quantifiable differences in porosity are seen through SEM images, then we hypothesize that these structural differences should lead to measurable changes in mechanical properties. However, the batch-to-batch variability of this biopolymer solution on resulting data will impact these conclusions and the ability to decouple the pore architecture from the silk concentration.

3.1.1 | Young's modulus is largely independent of polymer concentration shifts within 3%–5% and changes in freezing rate

Given the observed differences in architecture, we sought to evaluate the influence of polymer concentration and porosity on static mechanical properties, specifically under uniaxial tension. Although isotropic silk fibroin sponges have been comprehensively studied under both compression and extension,[5] previous reports on anisotropic sponges only report mechanical properties assessed under compression.[1] For applications relevant to muscle, hydrated tensile testing of the anisotropic sponges is more relevant. From each of the different sponge formulations (Table 1), two sample sponges were cut from the bulk of three different sponges generated ($n = 6$) to demonstrate reproducibility during sponge generation (two biological replicates for each of the three technical replicates). To assess static bulk tensile mechanical properties, the Young's modulus was calculated from the linear viscoelastic region of the extensional stress strain curve (Figure 2E) between strains of 0%–3% (see Figure S3), as there was no toe-region at low strain amplitudes and this strain region had the best linearity across all formulations.[38,39] The relative shape of the stress–strain curves were similar for the fabrication parameters in

Figure 2E demonstrating similar behavior to elastomeric materials.[38] The material also exhibits ductile fracture after a period of plastic deformation at high strain rates.[38] The bulk tensile properties were assessed at two strain rates, 1% strain per minute and 10% strain per minute, as these are relevant rates for native skeletal muscle.[40,41] The first important result is that, for all silk fibroin sponge formulations, the rate of deformation utilized in this work, did not significantly impact the measured static mechanical property value (respective filled in vs. open bars in Figure 2F vs. Figure 2G).

Results show that despite the obvious observed differences in the pore architecture (vertical comparisons, Figure 2A vs. Figure 2C and Figure 2B vs. Figure 2D), the calculated Young's modulus is statistically similar across both silk fibroin concentrations at both strain amplitudes (comparing circles to squares in Figure 2F for 1% strain per minute and Figure 2G for 10% strain per minute, $.99 < p < .54$). However, when comparing the freezing rate, use of 50% ethanol to achieve a slower rate of freezing was different from use of 100% ethanol ($p < .1$) at 1% strain per minute suggesting that there is some influence of the freezing rate and resulting pore size on the calculated Young's modulus at 5% silk fibroin, where greater polymer entanglement is expected during the sample freezing (comparing yellow to blue squares in Figure 2F for 1% strain per minute and Figure 2G for 10% strain per minute). This trend does not hold at 10% strain per minute where the same comparison at 5% is similar ($p = .47$), suggesting that these changes in pore architecture only impact deformation at low strain amplitudes and instead, at higher strain amplitudes these differences actually result in larger sample to sample variability. Across all other comparisons for Young's modulus at 10% strain per minute, the freezing rate does not have a significant impact on this tensile mechanical assessment ($.47 < p < .99$).

3.1.2 | Impact of silk concentration and freezing rate on ultimate tensile strength

Similarly, we evaluated the impact of silk concentration and freezing rate on UTS, again showing that strain amplitude did not significantly impact the resulting average UTS for a given sponge formulation (respective filled in vs. open bars in Figure 2H vs. Figure 2I $p > .95$ with values provided in Table S2). Values for the UTS were on the order of 200–500 kPa, with average error in these measurements on the order of 50–100 kPa (values provided in Table S2). In addition, freezing rate had no impact on UTS in 3% silk sponges which was around 200–300 kPa, which is not surprising given the similarities between the silk fibroin sponge structures in Figure 2A and Figure 2B. However, at 1% strain per minute, there was a significant difference between the UTS of 3% and 5% silk fibroin sponges formed with 100% ethanol ($p = .018$, 200–300 kPa vs. 350–500 kPa, respectively, with values provided in Table S2). Additionally, 5% silk fibroin sponges formed at 50% ethanol and 100% ethanol were statistically different ($p = .006$), ranging from around 275 kPa (50% ethanol) to 400 kPa (100% ethanol). These trends suggest that UTS increases with increasing silk concentration and faster freezing rates when assessed at 1% strain per minute. However, these trends disappear in the 10% strain per minute analyses as the variability in these measurements increases.

3.2 | Method of induction of crystallinity alters crystalline content

Silk fibroin forms a tertiary structure through interactions between the heavy and the light chains within the class of silk fibroin proteins. These tertiary structures are driven by the exclusion of water from the backbone of the heavy chain, resulting in the formation of beta-sheet structures.[42–44] These beta-sheet structures then form crystal structures through the coming together of these individual beta-sheets into larger structures. This process is driven by thermodynamics and the rate of water exclusion and the energy in the system can be controlled through temperature and pressure, resulting in the formation of water insoluble silk materials.[24] Previously, results have shown that the method used to drive out water, form beta-sheets, and come together to make crystal structures can be modulated using different post-lyophilization methods, such as water annealing (room temperature, under vacuum) or autoclaving (high temperature, atmospheric pressure).[23,24] For isotropic sponges, it has been shown that for sponges made with no crystallinity induction steps, there is negligible beta-sheet content as compared to 6-h water annealed sponges.[8] Additionally, it has been shown that for isotropic sponges, increasing the crystallinity content increases the Young's modulus and UTS through tensile mechanical testing and we hypothesized that our anisotropic sponges would have a similar trend due to crystallinity content.[5] Here, we aim to understand if the method used to induce crystallinity has an impact on static tensile mechanical properties. Figure 3 shows the difference in static tensile mechanical properties as a function of the method for inducing crystallinity for both 3% and 5% silk sponges at our faster freezing rate conditions (100% ethanol slurry).

3.2.1 | Young's modulus is independent of crystalline content

Based on observations from SEM images, it appears that autoclaved samples show differences in pore structure, with changes in the relative distances between silk sheets observed for both 3% and 5% silk (horizonal comparisons, Figure 3A vs. Figure 3B and Figure 3C vs. Figure 3D). Young's moduli, calculated from the slope of the stress–strain curve (Figure 3E), are shown in Figure 3F–I. The representative stress–strain curves (Figure 3E) for the autoclaved samples and the water annealed samples show shifts in characteristic shape.[38] The stress–strain curves for the autoclaved samples start out with elastomeric behavior, but then show some similarities to a semi-crystalline material that undergoes plastic deformation at high strains. However, the water annealed samples show elastomeric like behavior over the range of strains evaluated. The autoclaved samples experience more brittle-like fracture as the strain amplitude increases,[38]

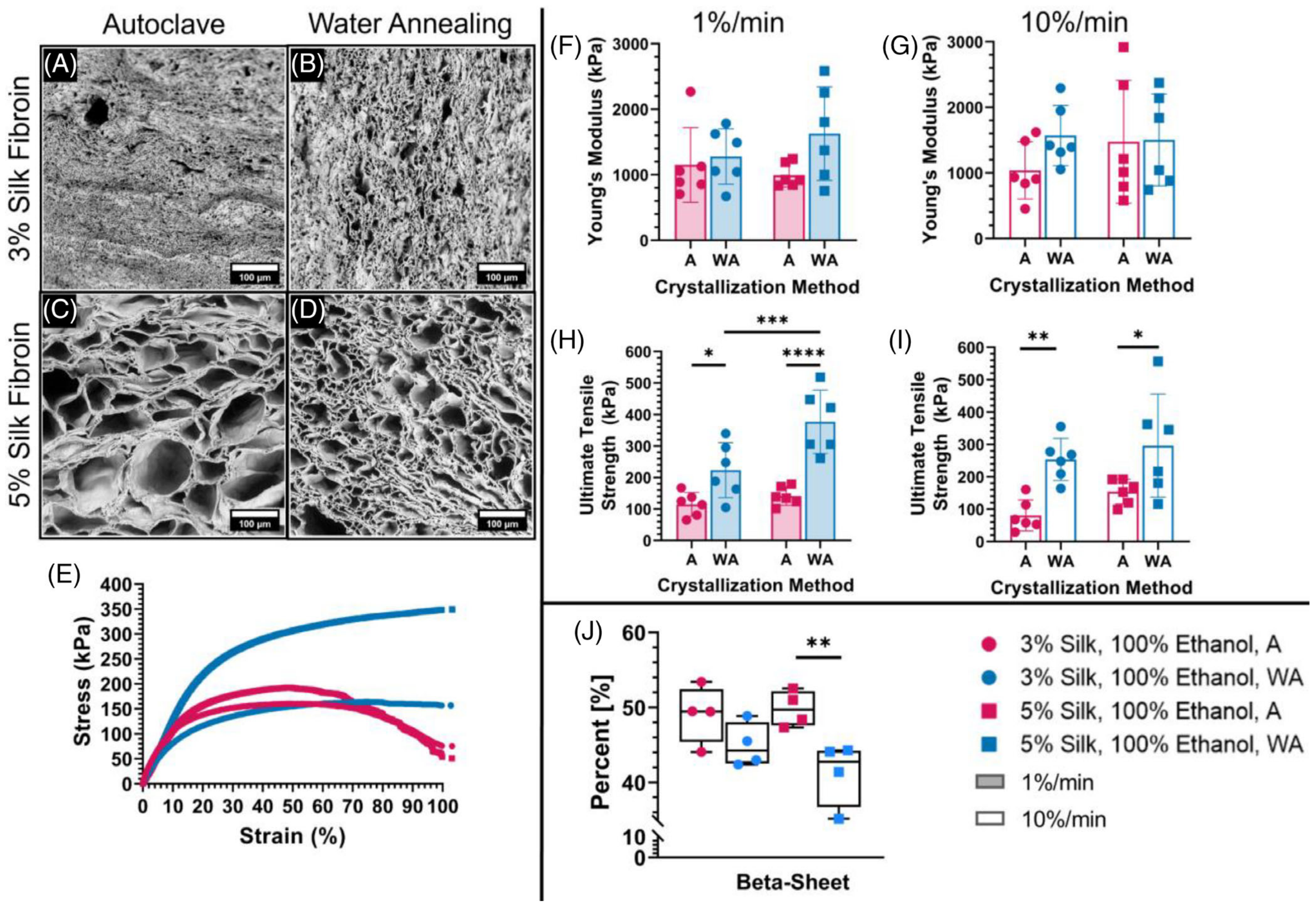

FIGURE 3 Structural images and static mechanical properties of anisotropic silk fibroin sponges formed with different silk concentrations and crystallinity induction (A–D) scanning electron microscopy cross-sections into the direction of alignment of sponges formed with different fabrication parameters (A) 3% silk fibroin concentration, 100% ethanol freezing solution, and autoclaving (B) 3% silk fibroin concentration, 100% ethanol freezing solution, and 6-h water annealing (C) 5% silk fibroin concentration, 100% ethanol freezing solution, and autoclaving (D) 5% silk fibroin concentration, 100% ethanol freezing solution, and 6-h water annealing. (E) Representative stress–strain curves at a rate of 10% strain per minute. (F–G) Average Young's modulus values for different sponge fabrication parameters ($n = 6$) (F) 1% strain per minute, (G) 10% strain per minute. (H–I) Average ultimate tensile strength values for different sponge fabrication parameters ($n = 6$) (H) 1% strain per minute, (I) 10% strain per minute. (J) Quantification of deconvoluted FTIR spectra for beta-sheet crystallinity regions known for *Bombyx mori* silk ($n = 4$). Data are expressed as mean ± standard deviation. Analyzed with 1-way ANOVA with Tukey's test post hoc analysis. Statistical significance is reported as $*p < .1$; $**p < .05$; $***p < .01$; and $****p < .001$.

resulting in a dramatic change in slope of the stress–strain curve at high amplitudes. At high strain amplitudes, the autoclave samples experience irreversible plastic deformation.

Similar to the Young's modulus comparisons made for shifts in freezing rate, there is no statistical difference between respective samples at 1% strain per minute versus 10% strain per minute for different methods of inducing crystallinity (respective filled in vs. open bars in Figure 3F and Figure 3G, $.85 < p < .99$). The average Young's modulus values for these sponges ranges from 1000 to 1600 kPa (Table S2), which aligns with the upper range of native skeletal muscle tissue Young's modulus.[40,41] In addition, results show that there is no significant influence of silk concentration or method of crystalline induction on the measured Young's modulus (Figure 3F and Figure 3G, $.17 < p < .99$). These results are consistent with previously reported results for similar isotropic silk sponges formed with *Bombyx mori* silk fibroin extracted for 30 min.[5]

To interpret these data, analysis of beta-sheet content was calculated from FTIR spectroscopy (see Figure S2). Data shows that autoclaved samples have an average of 50% beta-sheet content whereas 6-h water annealed anisotropic silk sponges have an average of 41% beta-sheet content (Figure 3J). Significant differences are found for the beta-sheet content of the 5% silk sponges when using different crystallization methods ($p = .019$). Based on our interpretation of FTIR using previously published deconvolution methods,[29] this suggests that the 5% silk fibroin autoclaved samples have greater crystalline content compared with the 5% silk fibroin 6-h water annealed samples. These results suggest that as the silk fibroin protein content increases, and polymer entanglement has a greater impact on the process of beta-sheet formation, then the tensile mechanical properties will change. These differences are not as pronounced as what has been observed in isotropic sponge formation, where the influence of the pore architecture may be less impactful.[5] However, FTIR deconvolution methods do not speak to the structure or size of the crystals formed between these two methods. We hypothesize that both total crystalline content as well as crystal size may influence static tensile mechanical properties, and depending on these structures, the strain amplitude may also influence resulting properties. As crystalline content increases, greater plastic deformation would be expected as the autoclave response more closely mimics a biphasic material.[38]

3.2.2 | Crystalline content has a significant impact on the ultimate tensile strength of anisotropic silk fibroin sponges

However, the influence of crystal structure and silk fibroin concentration are significant in the analysis of UTS. First, it should be noted that data shown in blue in Figure 3 are the same data shown in blue in the corresponding in Figure 2; thus, silk fibroin samples formed with 100% ethanol during freezing and water annealed for 6 h are shown in blue. This data set is compared to the pink samples (Figure 3), which were formed with 100% ethanol during freezing and autoclaved to induce crystallinity as opposed to water annealed. Results show that for the calculation of UTS, crystalline structure and method of crystal formation are significant. Across all conditions, the respective autoclaved samples are statistically different from the concentration and strain amplitude matched formulation (Figure 3H $p < .07$ and Figure 3I $p < .06$). Surprisingly, even though the autoclaved sample contains higher crystalline content, the UTS is lower compared with water annealed samples. The size of these crystal structures may impact the viscoelastic properties and start to instead exhibit plastic deformation.

Similarly, our results in Figure 3F,G align with trends in the literature that suggest that 3% silk fibroin sponges do not show significant differences in the Young's modulus when comparing autoclaving and water annealing as the method of crystal formation within the silk fibroin sponges.[5] The anisotropy is not the driving force in this comparison as trends in Young's modulus reported previously in isotropic sponges[5] hold within our anisotropic materials. Anisotropic silk fibroin sponges show significant differences in UTS between different post-lyophilization methods, which deviates from previous work for isotropic sponges.[5]

3.3 | Implications of crystal structure, size, and organization on measured mechanical properties

Furthermore, Figure 3E shows substantial variation between crystallization methods at high strain rates. Althoughthese strain rates may not be critical for use of this material for long-term tissue culture platforms, it is significant should these materials be implanted into the body, as strains are harder to predict and control upon implantation as they are dependent on the tightness of the interface between the implanted material the host tissue. Therefore, we sought to phenomenologically understand if crystal structure could drive these differences in deformation at high strain amplitudes. To do this, we used MD simulations to model two systems with different crystalline organization to correlate computational results with data given in Figure 3E. We hypothesize from our observed mechanical characterization data of these aligned silk sponges that the changes in viscoelastic behavior at high strain amplitudes are due to the organization of the crystalline domains within the secondary structure of the silk fibroin polymer as the post-lyophilization methods produce the most significant differences in viscoelastic behavior. These post-lyophilization methods thermodynamically drive the formation and organization of crystalline regions of the fibroin heavy chain. The crystalline regions are connected through elastic amorphous regions from the fibroin light chain and overall size of the crystal structure will be dependent upon the driving forces for crystal formation (e.g., pressure, temperature) as water is excluded from the backbone.[24,45] Although we quantified the total crystalline content through FTIR analysis[24,29] of beta-sheet content (Figure 3J), we cannot elucidate the organization or size of these crystalline regions throughout these systems.

Results from MD simulations are presented in Figure 4, in which the mechanical response of the amorphous and crystalline regions of the silk fibroin polymer are evaluated. We hypothesized that the size of the crystalline regions drive the high strain amplitude behavior, as previously described in synthetic crystalline polymer literature.[38] Thus, we created systems with two different silk biopolymer domains, representing the amorphous and crystalline regions, varying the size and ratio of these regions to elucidate the role of silk fibroin crystal size relative to the amorphous region on high strain rate mechanical properties. We simulated these biopolymers such that four chains are stacked on top of each other per simulation box (Figure S7).

Chain A (pink structure) is comprised of larger crystalline domains (23.5 kDa) and Chain B (blue structure) has four smaller crystalline domains (9.4 kDa). Both chains have comparable total molecular weights, 236 and 230 kDa, for chain A and B, respectively (Figure 4A). Tensile deformation of the chains was applied in the *z* direction, along the longest axis, at three different rates. The proposed strain rates of $25 \times 10^9\ \text{sec}^{-1}$ (Figure 4B), $50 \times 10^9\ \text{sec}^{-1}$ (Figure 4C), and $100 \times 10^9\ \text{sec}^{-1}$ (Figure 4D) are similar order of magnitude strain rates that have been successfully applied to MD deformation studies.[26,46] Video S2 shows the stretching of the silk fibroin chains where the amorphous regions are being stretched and deformed whereas the crystalline regions resist deformation due to their high organizational structure.

The larger crystalline region has an impact on the stability of chain A; but, as soon as it reaches strains larger than its yield point, they experience rapid, irreversible deformation as shown in the stress–strain curves (chain A, pink in Figure 4B). This result, and observed permanent plastic deformation, aligns with the measured stress–strain response of the autoclaved anisotropic silk sponges (pink curves, Figure 3E). Comparatively, chain B (Figure 4B, blue) shows a viscoelastic response, similar to that found in Figure 3E for the water annealed anisotropic silk sponges (blue curves). In this phenomenological model,

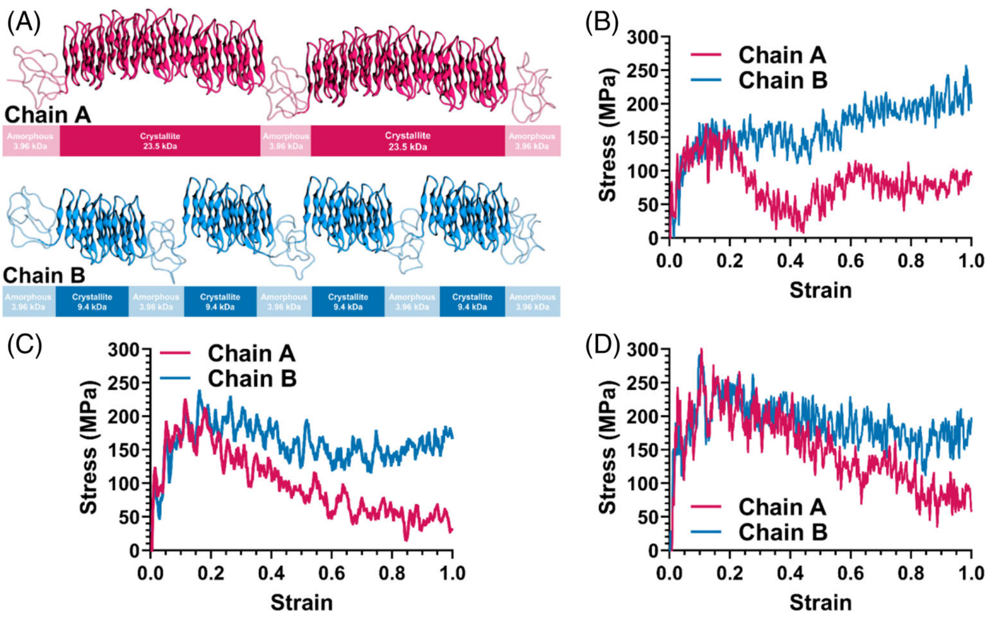

FIGURE 4 Results of static stretching of silk protein chains with different crystallinity organization. (A) Structure of chain A in pink and chain B in blue. (B) Representative stress–strain curve of chain A and chain B at a rate of 25 × 10^9 sec^{-1}. (C) Representative stress–strain curve of chain A and chain B at a rate of 50 × 10^9 sec^{-1}. (d) Representative stress–strain curve of chain A and chain B at a rate of 100 × 10^9 sec^{-1}.

chain B exhibits an elastomeric response that increases with increasing strain and does not appear to experience permanent deformation, which begins to allow us to make hypotheses about the role crystallization method plays in resulting crystal size and organization within the sponges. The strain rate of 50 × 10^9 sec^{-1} (Figure 4C) demonstrates a similar response to the 25 × 10^9 sec^{-1} (Figure 4B), but with not as dramatic of a change in slope for chain A. There still appears to be more plastic deformation in chain A than chain B. Similarly, in Figure 4D, for the strain rate of 100 × 10^9 sec^{-1}, the two different polymer chains exhibit similar stress–strain responses at low strain with some deformation of chain A at higher strains.

Based on these results, we can confidently hypothesize that the driving force of these stress–strain responses in our experimental data are the different organization of beta-sheet crystals in the aligned silk fibroin sponges due to the different post-lyophilization methods that induce crystallinity. This corresponds to the MD simulations where chain A mimics the experimental response of the autoclaved sponges and chain B mimics the experimental response of the water annealed sponges. We hypothesize that the change in temperature of these post-lyophilization processes drive the formation and structure of the crystalline domains seen in Figure 4A. The autoclave method occurs for approximately 30 min at high temperature (120°C) and atmospheric pressure (0.101 MPa) whereas the water annealing method occurs at room temperature (23°C) under vacuum conditions (0.0233 MPa) for 6 h. The difference in time, temperature, and pressure of these post-lyophilization methods thermodynamically drives the organization of the crystalline regions. Since chain A exhibits a similar response to our autoclaved sponges, we hypothesize that the higher temperature drives the formation of larger crystalline domains. Conversely, the vacuum and room temperature conditions of the water annealing are hypothesized to produce smaller more frequent regions of crystallinity in the secondary structure. These hypothesized structures are instrumental in understanding the driving forces behind the crystallinity-inducing methods and their impact on the resulting mechanical responses of the aligned silk fibroin sponges.

3.4 | Dynamic tensile mechanical property analysis

Although the static mechanical properties are important for understanding the overall bulk response of the material at a set strain rate, static testing does not give insight into the time dependent response of the material. For the applications of this material, we are interested in long-term response and therefore utilized oscillatory tensile testing for information about the viscoelastic behavior of the sponges at different formulations. For determining the effect of frequency and amplitude on the sponges, oscillatory tensile sweeps were performed. Amplitude sweeps were performed first to understand the linear regime of elastic deformation. The tensile amplitude sweeps were performed at 1 Hz from a range of 0% strain amplitude through 100% strain amplitude, however most sponges could not reach 100% elongation and ruptured by around 60% strain amplitude (Figure 5A and Figure 6A, see Figure S4). Frequency sweeps were conducted at a constant strain amplitude of 10% and frequencies from 0.2 to 10 Hz (Figure 5F and Figure 6F, see Figure S5). The constant amplitude value was chosen based on the evaluation of the yield point of the silk fibroin sponges since the linearity of the material response begins to deviate after 10% strain amplitudes for most samples. For all amplitude and frequency sweeps, the storage modulus is always greater than the loss modulus, demonstrating the response of a viscoelastic solid material. The frequency sweep trends start to decline as the frequency increases to 10 Hz due to the limitations of our experimental apparatus. All tensile testing for these results is done on a rheometer equipped with dynamic mechanical analyzer capabilities. This set-up includes an external cup that fits around the testing apparatus that is filled with ultrapure water. As the frequency of the test increases, the

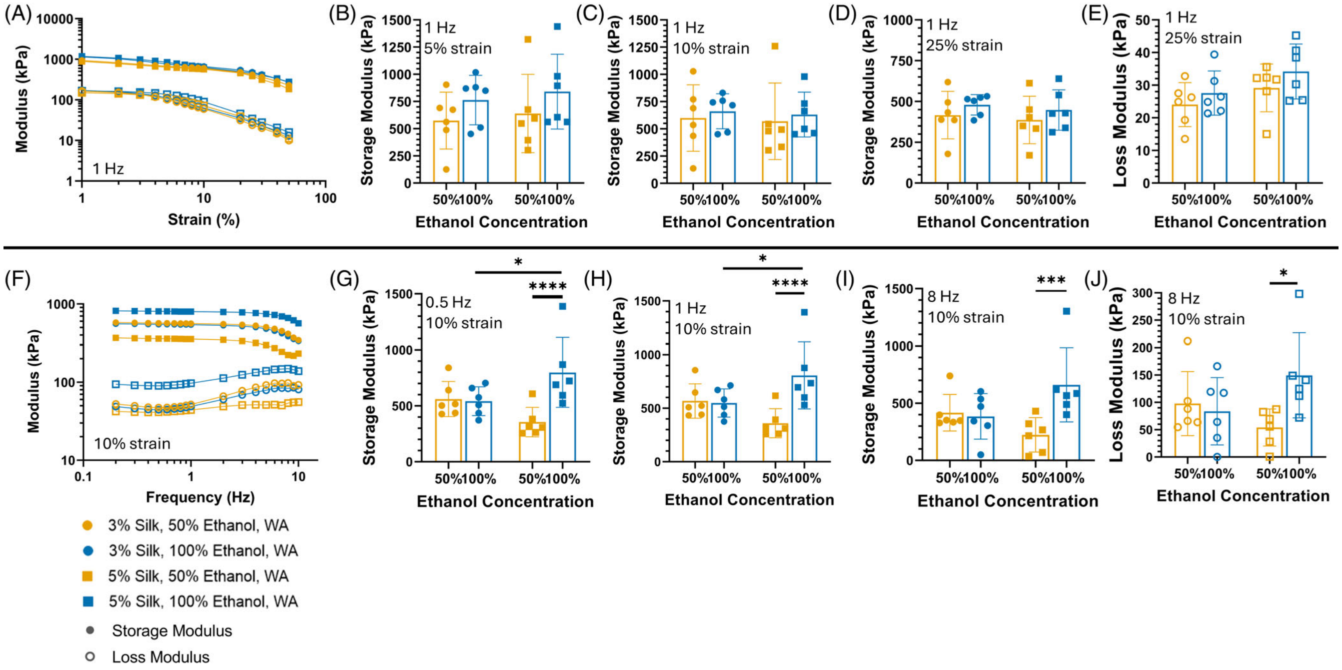

FIGURE 5 Dynamic mechanical properties of anisotropic silk fibroin sponges formed with different silk concentrations and freezing rates. (A–E) Amplitude sweeps ($n = 6$). (A) Mean amplitude sweep from 0% strain to breakage at constant 1 Hz frequency. (B) Storage modulus values at 5% strain and 1 Hz. (C) Storage modulus values at 10% strain and 1 Hz. (D) Storage modulus values at 25% strain and 1 Hz. (E) Loss modulus values at 25% strain and 1 Hz. (F–J) Frequency sweeps ($n = 6$). (F) Mean frequency sweep from 0.2 to 10 Hz at constant strain amplitude of 10%. (G) Storage modulus values at 10% strain and 0.5 Hz. (H) Storage modulus values at 10% strain and 1 Hz. (I) Storage modulus values at 10% strain and 8 Hz. (J) Loss modulus values at 10% strain and 8 Hz. Data are expressed as mean ± standard deviation unless otherwise stated. Analyzed with 1-way ANOVA with Tukey's test post hoc analysis. Statistical significance is reported as $^*p < .1$; $^{***}p < .01$; and $^{****}p < .001$.

water begins to slosh in the cup resulting in artifacts in the modulus values due to the forces of the water distribution in the cup. We attribute the nonlinearity at high frequencies to the experimental apparatus and not the failure of the material.

3.4.1 | Dynamic response of silk sponges as a function of silk fibroin concentration and freezing rate

Similar to the Young's modulus and UTS analysis, we first looked at the response of silk fibroin concentration and freezing rate on the viscoelastic response of the sponges. The average amplitude sweeps for changing concentration and freezing rate (Figure 5A) shows great agreement qualitatively in shape and quantitatively in storage and loss modulus values. The distance between the storage and loss modulus values does not change through the different strain amplitude values. Figure 5B–D shows individual points and statistics for low, medium, and high amplitude values. The storage modulus values for different silk fibroin concentrations (3% and 5% silk) at 1 Hz frequency and 5% strain amplitude (Figure 5B), at 1 Hz frequency and 10% strain amplitude (Figure 5C), and at 1 Hz frequency and 25% strain amplitude (Figure 5D) are statistically similar ($.67 < p < .99$). We also report the loss modulus values at 1 Hz frequency and 25% strain amplitude (Figure 5E) exhibit statistical similarity ($.45 < p < .92$) to the loss modulus values as well. This similarity demonstrates that the oscillatory amplitude response of the sponges is not dependent on silk fibroin concentration at 3% and 5% as well as freezing rates developed with 50% ethanol and 100% ethanol freezing slurries.

For the frequency sweeps, there were greater differences in modulus values for differences in silk concentration and freezing rate. The average frequency sweeps (Figure 5F) for different silk fibroin concentrations and freezing rates remain linear up to 2 Hz frequency, after which they begin to have changes in slope. The changes between silk fibroin concentrations and freezing rates are more prominent in the frequency sweep versus the amplitude sweeps for these samples. For changes in freezing rates, the 3% silk fibroin shows statistical similarity for both freezing conditions ($p > .999$). However, for the 5% silk fibroin concentrations, there are statistical differences between the different freezing conditions. For comparison at a low frequency of 0.5 Hz and medium frequency of 1 Hz (Figure 5G,H), the storage modulus at 5% silk is statistically significant between 50% ethanol and 100% ethanol freezing conditions ($p < .0001$ and $p < .001$, respectively). The storage modulus at 8 Hz (Figure 5I) also shows statistical significance between freezing conditions with 5% silk fibroin concentration ($p < .007$). The loss modulus at 8 Hz also shows statistical differences ($p = .054$) between the freezing rates of the 5% silk, although not as significantly, demonstrating that the storage modulus dominates this material response. This reduction in significance is hypothesized to be due to the increase in spread of the data points due to the apparatus limitations

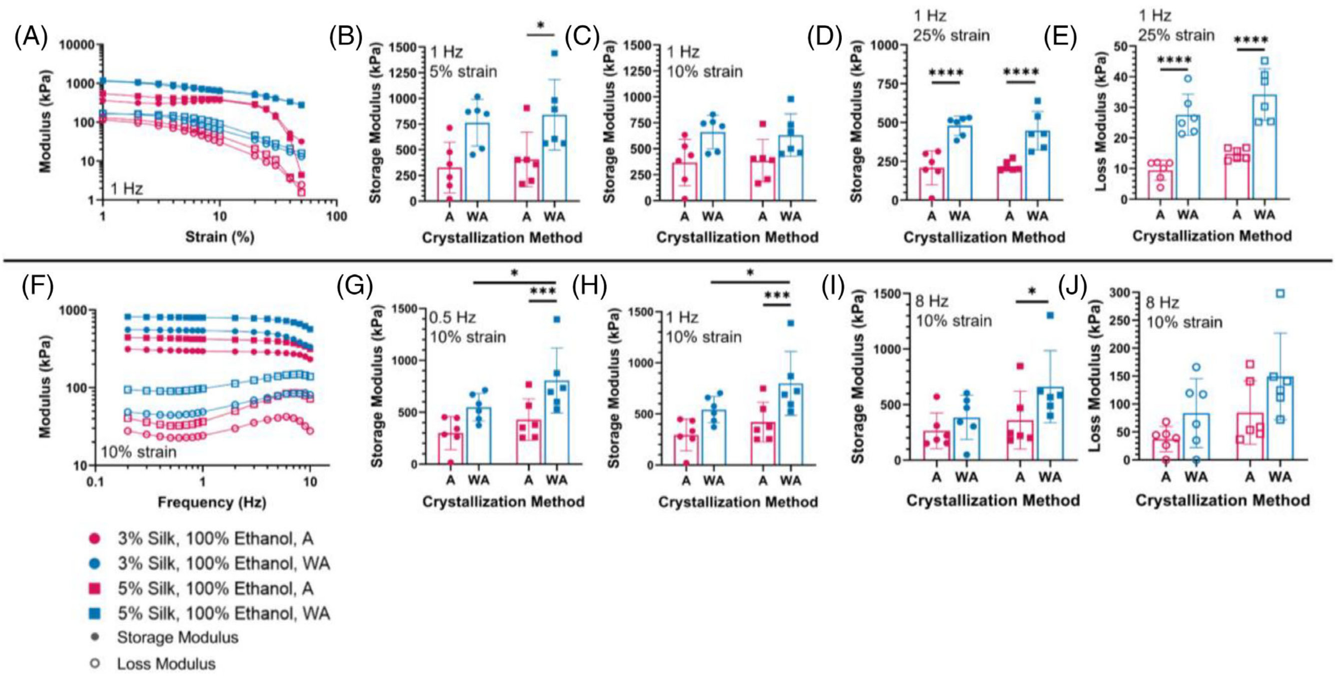

FIGURE 6 Dynamic mechanical properties of anisotropic silk fibroin sponges formed with different silk concentrations and crystallinity induction (A–E) Amplitude sweeps ($n = 6$). (A) Mean amplitude sweep from 0% strain to breakage at constant 1 Hz frequency. (B) Storage modulus values at 5% strain and 1 Hz. (C) Storage modulus values at 10% strain and 1 Hz. (D) Storage modulus values at 25% strain and 1 Hz. (E) Loss modulus values at 25% strain and 1 Hz. (F–J) Frequency sweeps ($n = 6$). (F) Mean frequency sweep from 0.2 to 10 Hz at constant strain amplitude of 10%. (G) Storage modulus values at 10% strain and 0.5 Hz. (H) Storage modulus values at 10% strain and 1 Hz. (I) Storage modulus values at 10% strain and 8 Hz. (J) Loss modulus values at 10% strain and 8 Hz. Data are expressed as mean ± standard deviation unless otherwise stated. Analyzed with 1-way ANOVA with Tukey's test post hoc analysis. Statistical significance is reported as $^{*}p < .1$; $^{***}p < .01$; and $^{****}p < .001$.

at high frequencies. There is also some statistical difference at low frequencies for the comparison of different silk concentrations with 100% ethanol freezing solution. Storage modulus for 3% and 5% silk at 100% ethanol shows significance at 0.5 Hz (Figure 5G) and 1 Hz (Figure 5H) ($.071 < p < .78$). The frequency dependence of this anisotropic silk fibroin sponges is greatest at low frequency values (<2 Hz), mimicking the material response to slower strain rates (1%/min) found through the static tensile tests.

3.4.2 | Crystalline content increases the linear viscoelastic range of anisotropic silk fibroin sponges

From the results of Figure 3, we expected that the crystallinity method would provide the greatest change in dynamic tensile mechanical properties over the other fabrication parameters. Again, the water annealed samples (blue data points in Figure 6) are the same as those shown in Figure 5. The mean amplitude sweeps for 3% and 5% silk concentrations with different crystallinity methods (blue vs. pink data points) are shown in Figure 6A. Much like the static stress–strain curves (Figure 3E), the autoclaved samples show greater qualitative change in their shape and lower qualitative modulus values than the water annealed samples. The autoclaved samples slope changes greatly at high strain amplitude values; however, they also have a larger linear elastic deformation range compared with the water annealed samples. Additionally, although the distance between the storage and loss modulus is constant for the water annealed samples, the autoclaved samples show differences in the storage and loss modulus shapes. The storage modulus at high strain amplitudes becomes similar in value to the loss modulus and begins to approach a gel point (equivalent storage and loss modulus),[47] due to the fracturing of the material, but do not reach it before complete breakage. Although the sample is fractured and close to breaking at high strains, the change in viscoelastic behavior is hypothesized to be due to the realignment and deformation of the amorphous regions[38] after the amorphous regions have been stretched to their maximum length. The higher amount of crystalline content has a more immediate impact on the stability of the autoclave samples; as soon as they reach strains larger than their yield point, they experience rapid, irreversible deformation.

Representative storage moduli at low, medium, and high strains of 5%, 10%, and 25% strain amplitudes show some significance between different crystallinity methods (Figure 6B–D). At 5% strain (Figure 6B), the 5% silk fibroin shows significant differences between the water annealed and autoclaved groups ($p < .025$). At 25% strain amplitude (Figure 6D), the different crystallinity methods show statistical significance for 3% silk fibroin ($p < .0001$) and for 5% silk fibroin ($p < .003$). Unlike other results, the autoclaved data points are tighter and more compact at higher strain values. The loss modulus (Figure 6E) shows similar statistical significance to the storage modulus at 25% strain amplitude. These anisotropic silk fibroin sponges are mostly dependent on strain displacement as shown from the mean amplitude sweeps. The linear elastic region is of great importance to the long-term performance of these sponges under mechanical stimulation. The maximum strain amplitude for any long-term culture applications should be maintained below the yield point of this material (<10%) for long lasting use. Below this yield point, the viscoelastic behavior is dominated by its elastic, reversible response. The extent of this elastic response will be explored through hysteresis testing.

The mean frequency response of the autoclaved sponges (Figure 6F) shows a similar qualitative response with minimal deviations from linearity at lower frequency values. Qualitatively, the modulus values of the autoclaved sponges are smaller than the water annealed ones, matching the trend in the static tensile test results. Again, the strong linear response of the modulus to changes in frequency demonstrates that the anisotropic silk materials respond independently of frequency within the linear elastic region. At lower frequency values of 0.5 (Figure 6G) and 1 Hz (Figure 6H), the change in crystalline content plays a large role in the mechanical response. The difference between crystallinity methods of 5% silk sponges is statistically significant ($p < .0008$ and $p < .0006$). At higher frequency values, the spread in data points increases due to the impact of the hydration in our experimental setup. Therefore, the statistical significance of the higher frequency modulus values (Figure 6I) is limited to significance between the crystallinity methods for the 5% silk fibroin sponges ($p < .07$). There are no statistical differences between loss modulus values at 8 Hz (Figure 6J) ($.344 < p < .691$) due to the wide spread of data at higher frequency values. Since these silk fibroin sponges are not largely dependent on frequency within their linear elastic region, the sponges can be applied to many different applications where the speed of oscillation of the mechanical stimulation can change for a given tissue.

3.5 | Long-term stability and viscoelastic response of anisotropic silk fibroin sponges

One of the drawbacks to many tissue engineering materials is their long-term performance. Specifically for in vitro models of skeletal muscle tissues, culture conditions only tend to last for short time periods (<6 weeks).[48–51] Longer time periods would allow for further differentiation and maturation to explore cell function and phenotype. For example, allowing for longer culture time in skeletal muscle modeling provides more time for maturation and the development of contractile tissue that many current models cannot obtain. To determine viability and stability of silk fibroin sponges as a long-term culture platform, we looked to perform long-term analysis under cyclic strain.

The goal of this investigation is to understand and capture sponge performance over time to inform the stability and bulk mechanical properties for future culture experiments. Hysteresis and fatigue tests were used to give insight into the long-term effects of cyclic strain on anisotropic silk sponges. Two representative sponges ($n = 1$) were chosen for long-term assessment. Because of the significant impact of crystallinity on static and dynamic tensile mechanical properties, 5% silk fibroin and 100% ethanol freezing concentrations were used to compare the long-term effects of water annealed and autoclaved sponges.

3.5.1 | Hysteresis and maintenance of mechanics over repeated cycles

Hysteresis shows the energy change upon loading and unloading a material, with the area between the curves as the energy lost during the deformation.[47] The material was extended from 0% strain to 10% strain at a rate of 10% per minute, then returned to 0% strain at the same rate. This process was repeated for 100 loops while the stress was recorded. The stress–strain curves (Figure 7A and Figure 7D) and calculated lost energy (Figure 7B and Figure 7E) are shown for the autoclaved and water annealed samples, respectively. The autoclaved hysteresis loops show wider loading and unloading curves with larger lost energy than the water annealed sponge. However, by loop 100, the autoclaved sample is able to fully close the loading and unloading curve such that they meet at zero strain (Figure 7A), representing a fully elastic response at these mechanical conditions. The water annealed sponge shows a narrower loading and unloading curves with less lost energy, but the loops are not able to unload back to zero strain over 100 loops (Figure 7D). The calculated lost energy shows a plateau after around 20 cycles of loading and unloading. These trends show that after an initial 10–20 cycles, sponges crystallized with either water annealing or autoclaving come to equilibrium when perturbed within the linear range (<10% strain). However, the lost energy, or inversely the stored energy, is different as a function of crystallization method. Thus, depending on the type or future application of these sponges, fabrication parameters should be carefully considered to ensure changes do not exist over the course of experimentation.

3.5.2 | Long-term stability assessed through cyclic fatigue testing

Fatigue tests were used to determine time dependent stability of the silk sponges as it is important for these sponges to be able to withstand mechanical perturbation over long culture periods. Fatigue tests were conducted at 10% strain amplitude and 1 Hz frequency for 6000 min. Both sponge types show similar trends in a constant, linear slope of storage modulus (Figure 7C and Figure 7F). The autoclaved sponge has a storage modulus plateau at around 376 kPa (Figure 7C) and the water annealed sample has a storage modulus of 642 kPa (Figure 7F). These storage modulus values correlate to the dynamic tensile tests where the water annealed sponges have larger modulus values than the autoclaving conditions (Figure 6). The loss modulus of

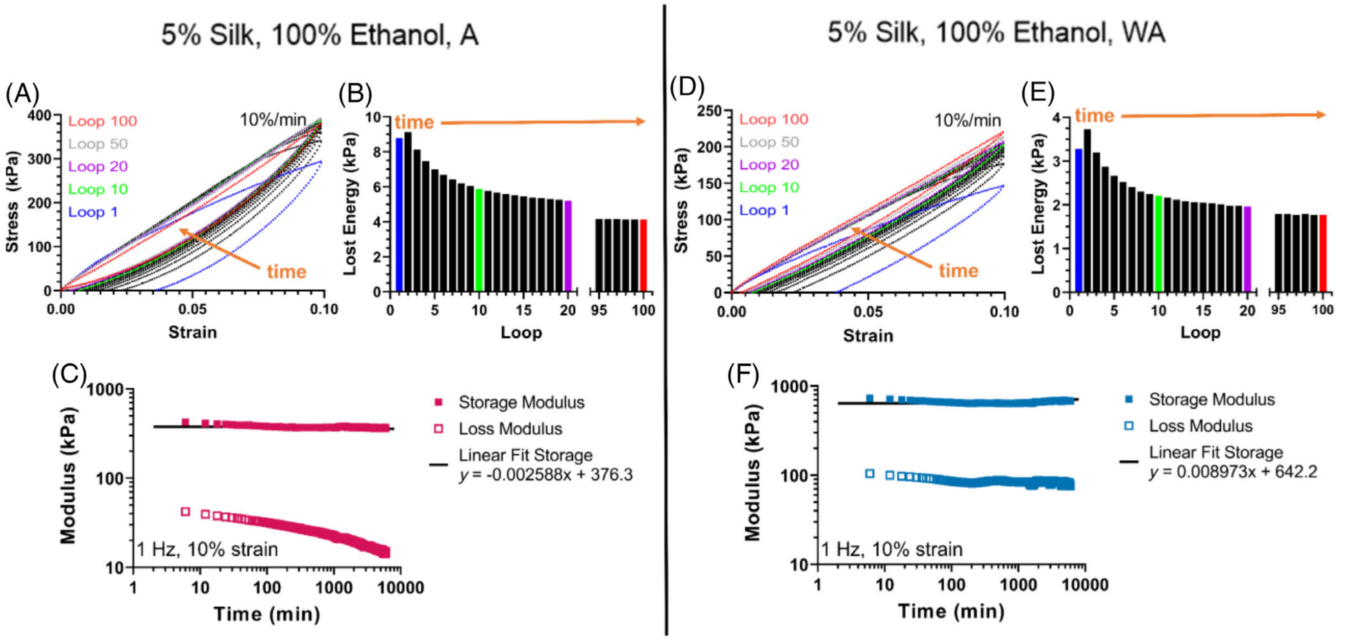

FIGURE 7 Long-term stability of anisotropic silk fibroin sponges (A–C) long-term stability of 5% silk fibroin concentration, 100% ethanol freezing solution, and autoclaving ($n = 1$). (A) Hysteresis analysis over 100 loops at 10% strain amplitude and 1 Hz frequency at a rate of 10% per minute, (B) lost energy of each hysteresis loop over 100 loops, (C) fatigue analysis via extensional testing at 10% strain amplitude and 1 Hz frequency for 6000 min. Linear fit denotes slope of the storage modulus (D–F) long-term stability of 5% silk fibroin concentration, 100% ethanol freezing solution, and autoclaving ($n = 1$) (D) hysteresis analysis over 100 loops at 10% strain amplitude and 1 Hz frequency at a rate of 10% per minute (E) lost energy of each hysteresis loop over 100 loops (F) fatigue analysis via extensional testing at 10% strain amplitude and 1 Hz frequency for 6000 min. Linear fit denotes slope of the storage modulus.

the two crystallinity methods differs. The water annealed sponge remains mostly constant throughout the 6000-min test. However, the autoclaved sample loss modulus slope declines throughout the test. This could be due to the interactions in the hydrated sample of bound water with the higher level of crystalline regions in the autoclaved sample compared with the water annealed crystallinity content.

Since we proved the material can undergo long-term perturbation (6000 min) with minimal change in storage modulus values, then it is hypothesized that it will be able to perform for several hours at a time with periods of rest in between as well. This shows good agreement with our hypothesis that within the linear range of the material, these anisotropic silk fibroin sponges have good potential to be utilized in long-term culture conditions that require mechanical perturbations. This linear slope is representative of a stable response of the sponges over time. Six thousand minutes of continuous perturbations are representative of culture conditions where long-term mechanical stimulation would be provided for 2 h per day for 8 weeks.

3.6 | Toward development of a long-term tissue culture platform using anisotropic silk sponges

After verifying the anisotropic silk fibroin system can withstand long-term perturbation, we moved toward more relevant environmental conditions of mechanical analysis. All prior mechanical property measurements were conducted fully hydrated in ultrapure water. However, this is not representative of the culture conditions this material would experience as a culture platform for seeding and maturation of cells. We also explored the influence of extracellular matrix physically entrapped in the anisotropic silk fibroin sponges, as this addition would give cells bioactive cues for adhesion and migration.[1] The addition of dECM has been previously assessed in this system through compressive mechanical testing,[1] but tensile testing has not previously been reported. In addition to mechanical properties, we assessed the 3D porosity of the anisotropic silk fibroin sponges. Although SEM and H&E staining can give cross-sectional views at different depths in the material, it is labor intensive and difficult to combine these cross-sections to gain insight into the 3D structure and interconnectivity of the pores. Nano-CT was utilized to view and assess the interconnectivity and tortuosity of the porosity as a function of post-lyophilization method.

3.6.1 | Impact of extracellular matrix and cell culture media on mechanics of anisotropic silk fibroin sponges

To examine the biologically relevant conditions this material might experience as an in vitro platform or in vivo implant, we performed the same static mechanical testing and fatigue analysis with the addition of dECM on hydrated samples in solutions of cell culture media. Adult porcine skeletal muscle dECM was utilized to make the material

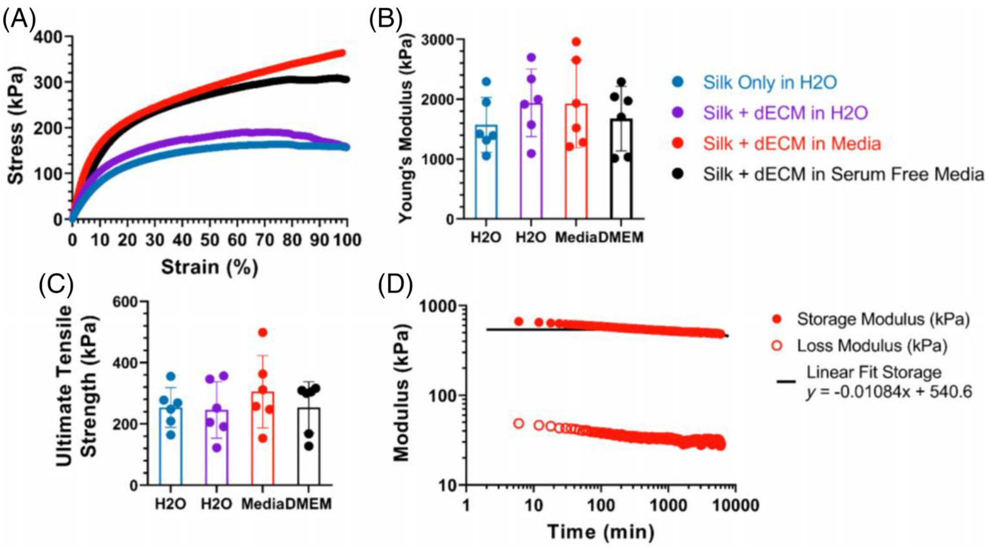

FIGURE 8 Static mechanical properties in different solutions of water, cell culture medium containing fetal bovine serum (FBS), or serum free cell culture medium for anisotropic silk fibroin sponges formed with 3% silk fibroin, 100% ethanol freezing solution, 6-h water annealing, and some with the addition of decellularized extracellular matrix. (A) Representative stress–strain curves at a rate of 10% strain per minute, (B) average Young's modulus values for different sponge fabrication parameters and hydrated solutions at 10% strain per minute ($n = 6$), (C) average ultimate tensile strength values for different sponge fabrication parameters and hydrated solutions at 10% strain per minute ($n = 6$). (D) Fatigue analysis via extensional testing at 10% strain amplitude and 1 Hz frequency for 6000 min for a sponge hydrated in cell culture medium containing FBS ($n = 1$). Linear fit denotes slope of the storage modulus. Data are expressed as mean ± standard deviation. Analyzed with 1-way ANOVA with Tukey's test post hoc analysis, with no significance found during the post hoc analysis.

relevant to skeletal muscle applications, but other ECM compositions could be utilized.[1] Reconstituted dECM was added to the silk fibroin solution before freezing the material. The silk fibroin sponges were hydrated in either ultrapure water, skeletal muscle growth medium containing FBS, or serum free Dulbecco's Modified Eagle's Medium (DMEM).

Since the results of Figure 2 and Figure 3 demonstrated that these aligned silk fibroin materials are not strongly rate dependent, we performed static mechanical testing at a rate of 10% per minute on the sponges with dECM. Representative stress–strain curves for each hydration solution and sponge with the addition of dECM can be seen in Figure 8A. The relative shape of the stress–strain curves, with the addition of dECM, was similar to that of the silk only fabrication (blue silk only samples are the same as Figure 2). This matches the results of similar compressive mechanical testing previously performed on anisotropic silk fibroin samples.[1] As previously described, the Young's modulus was calculated from the linear range of the stress strain curves. There are no significant differences ($p > .70$) in Young's modulus values (Figure 8B) for the addition of dECM or different hydration solutions. Upward trends suggest the potential influence of large serum proteins, such as those in FBS, in the analysis of mechanical properties, but these shifts are not statistically significant ($p > .88$). Figure 8C shows the values of UTS for the aligned sponges. Again, these values are not significantly different for the addition of dECM or different hydration solutions ($p > .77$). Thus, we can conclude that assessments performed in water at low strains (<10%) are sufficient to describe the behavior of that sample in relevant culture conditions.

With the long-term assessment from Figure 7, we wanted to confirm this long-term stability held with the addition of dECM and cell culture medium. The same fatigue test was performed for one representative sponge made with 3% silk fibroin, 0.2 mg/mL dECM, 100% ethanol, and 6-h water annealing. This sample was hydrated in serum containing cell culture medium and mechanically perturbed at 10% strain amplitude and 1 Hz frequency for 6000 min, shown in Figure 8D. The addition of dECM and use of cell culture media as the hydrating solution led to similar results to those presented in Figure 7, as noted by the similarities in the slope of the linear fit of the modulus values, which remain essentially zero (≤0.01). Therefore, we demonstrate that the addition of relevant extracellular matrix components and culture medium do not alter mechanical function or effect the long-term use of this material as a culture platform in bioreactors where strain amplitudes of <10% and frequencies of <2 Hz are commonly used.[52–55]

3.6.2 | Understanding the impact of scale-up and pore interconnectivity on diffusion and cell seeding as sponge size increases

Anisotropic silk fibroin scaffolds generated via ice templating have been previously utilized for in vivo studies in cardiac applications[1] and in vitro fibroblast compatibility assessments.[3] Previous work has shown that scaffolds of sizes of 10 mm by 5 mm by 2.5 mm[1] and 5 mm diameter by 2 mm thickness[3] have been successful for cell infiltration and proliferation. The mechanical assessments described in

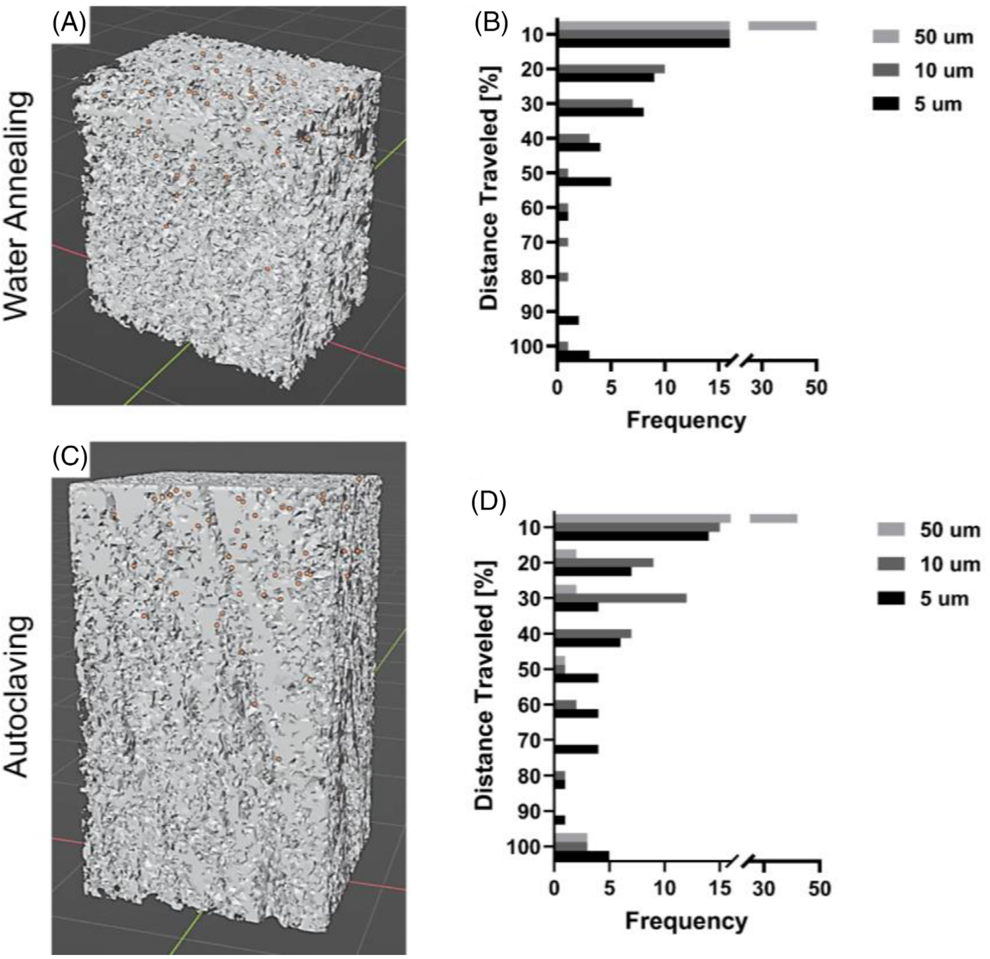

FIGURE 9 (A) 5% silk fibroin, 100% ethanol, and water annealed sponges simulated in blender with 50 spheres of 10 μm diameter (B) histogram of three different size spheres, 5, 10, and 50 μm traveled through the distance of the total sponge length in the direction of the aligned porosity of the water annealed sponge (C) 5% silk fibroin, 100% ethanol, and autoclaved sponge simulated in blender with 50 spheres of 10 μm diameter (D) histogram of three different size spheres, 5, 10, and 50 μm traveled through the distance of the total sponge length in the direction of the aligned porosity of the autoclaved sponge.

this work were conducted on 18 mm by 8 mm by 2 mm size sponges, slightly larger than those previously reported. Since these sponges are cut to size from a larger biomaterial (30 cm by 30 cm by 10 cm), this demonstrates the variety of sizes for potential applications of these aligned silk fibroin materials. Understanding the scale-up potential of this system for applications in skeletal muscle modeling may be of interest to look at bulk performance and functionality of larger sponge sizes.

Previous work on ice-templated silk fibroin sponges quantified pore size and wall thickness of different fabrication parameters,[3] but the implication of these changes are the overall tortuosity and interconnectivity of the porous structures. High interconnectivity will help in scale-up for larger sponges and achieve homogeneous cell infiltration. Given the differences in mechanical properties and hypothesized differences in crystal size and organization, we explored the tortuosity and interconnectivity of the pores as a function of post-lyophilization method on these parameters. Nano-CT was utilized to view the 3D architecture and computational assessments were used to look at spherical particle flow through the porous 3D structure. Small samples were cut from silk sponge strips and hydrated in iodine solution for contrast. After 24 h, the samples were rinsed to remove any excess contrasting agent from the pores and were scanned hydrated in ultrapure water to eliminate shrinking through drying.

The 5% silk fibroin and 100% ethanol sponges were used to compare post-lyophilization methods at 6-h water annealing and autoclaving ($n = 1$). Cross-sections and 3D renderings can be found in Figure S8. From the nano-CT renderings, the scans were converted into a 3D reference mesh. Taking inspiration from Qazi et al.,[56] we simulated dropping 50 spheres of three different diameters (5, 10, and 50 μm diameters) into the direction of alignment of the sponges (Video S3). These diameters were chosen to represent different size particles that could infiltrate the sponges, specifically that skeletal muscle cells will need to infiltrate and have room to mature and fuse into skeletal muscle fibers that can range in size from 10 to 100 μm.[57,58] Figure 9A–C shows the 10 μm size particles (in orange) falling through the two different sponge fabrications and the histograms (Figure 9B–D) shows where the particles are retained as a function of percent of the total length of the sponge.

A majority of all size particles are retained in the first 30%–40% of the sponge length. In both sponges, the 50 μm particles were unable to effectively penetrate the mesh network. We attribute this to the transition from the nano-CT rendering to the 3D mesh network, as the pore areas have been previously measured to be in the range of 100–90,000 μm^2.[3] The iodine solution necessary for contrast during the nano-CT scan had difficulties with homogenous distribution in the samples that may have affected the initial scans. The computational parameters could be further optimized in converting the scans to 3D meshes, but for an initial assessment into the interconnectivity of pores was successful in learning that the particle size did not necessarily dictate how far the particle could travel because even all of the smallest size particles could not traverse the entire length. The difference between the post-lyophilization methods showed the greatest difference in the 10 μm spheres, but overall, both water annealing and autoclaving have similar pore interconnectivity. Although further optimization of this analysis strategy could be completed, better translation of these aligned silk fibroin materials will be achieved through increasing pore interconnectivity. Previous work has shown that hollow arrayed channels can be incorporated into silk fibroin scaffolds to increase nutrient diffusion and cellular integration, often used perpendicular to pore alignment.[6] Further work would need to recharacterize the mechanical properties to ensure they are representative of skeletal muscle tissue the sponge is intended to mimic if the internal structure is significantly altered from normal aligned ice templated silk fibroin sponges.

4 | CONCLUSION

Development of long-term engineered tissue culture platforms necessitates a biomaterial that can maintain cell viability, promote and maintain cell maturation, and enable diffusion of key nutrients, growth factors, and O_2. To achieve these goals, many researchers have taken advantage of silk materials to support long-term in vitro studies.[2,10,11] However, long-term culture platforms that support engineered contractile muscle must also maintain an elastic or viscoelastic response over the course of the culture period, to ensure applied mechanical stimulation is in fact translating to the muscle cells or muscle fibers and activating mechanotransductive pathways. A long-term tissue culture platform for skeletal or cardiac muscle would need to support growth (1–2 weeks), maturation (∼4 weeks), and an experimental period where a hypothesis could be tested and the impact of a shift in culture conditions could be assessed (1–4 weeks), representing a need for 6 weeks in culture at a minimum. Sponge-like scaffolds made from silk fibroin have shown promise as short-term contractile muscle culture platforms and as implantable systems.[1,3] However, to utilize these materials for long-term (>6 weeks) platforms for the culture of contractile muscle, a full evaluation of the conditions under which these sponges can withstand repeated, dynamic mechanical perturbation was necessary.

In this work, we showed that anisotropic silk sponges remain tunable via control over initial formulation, as previously demonstrated with isotropic sponges[5] and previously shown via compression testing.[1] Hydrated static tensile mechanical properties vary as a function of evaluated formulation parameters, with the method by which protein crystallinity was induced having the greatest impact on static properties. These static mechanical properties show good agreement with native skeletal muscle mechanical properties.[40,41] Furthermore, we confirm that certain formulations of anisotropic silk sponges can undergo dynamic evaluation without a change or shift in sponge properties. Similarly, when silk protein crystallization and beta-sheet formation are induced via autoclaving the sponges exhibit more plastic-like deformation at higher strain rates and frequencies. Conversely, when protein crystallization and beta-sheet formation are induced by water annealing sponges maintain their elastomeric-like properties at higher strain rates and frequencies. MD results suggest that the driving force of the static mechanical response in our experimental data is due to different organization of beta-sheet crystalline domains. The difference in time, temperature, and pressure of the post-lyophilization methods thermodynamically drives the organization of the crystalline regions into large groupings (autoclaved experimental data) or smaller crystalline regions separated by flexible alpha-fold linkers (water annealed experimental data).

Moreover, we demonstrate that the aligned silk fibroin sponges are able to withstand dynamic mechanical perturbation over long-time scales, showing a plateau of the energy lost with each repeated cycle (hysteresis remains consistent over many cycles) and that the storage and loss moduli remain consistent following >6000 min of stretching in the linear regime at 1 Hz frequency and 10% strain amplitude. We further demonstrated that these properties persist when dECM is added to the sponge formulation and the tests are performed in serum-containing cell culture media. The lack of change and the presence of consistency highlight the utility of these sponges to serve as long-term tissue culture scaffolds for applications in contractile muscle evaluation. However, the results also show the unique challenges posed when using these materials such as pore interconnectivity, scale-up, and the influence of sterilization procedures[4,5] on bulk mechanical properties and polymer interactions. Moving forward, the application chosen for these materials will dictate whether or not autoclaving can be used as both a method of crystallization and sterilization,[4] or if another sterilization method, such as the use of ethylene oxide, gamma irradiation, or vaporized hydrogen peroxide, is preferred. Future work will need to build on previous reports[1,3] demonstrating short-term culture of contractile cells within these anisotropic materials for future applications in muscle tissue regeneration or as models of disease.

ACKNOWLEDGMENTS

To accomplish some of the reported analysis, including nano-CT imaging, we used the Research Service Centers of the Herbert Wertheim College of Engineering at the University of Florida with extremely valuable assistance from Gary Scheiffele, Ph.D. Additionally, we acknowledge University of Florida students Lauren Eccles, Travis Truong, and Llia Byron for support in silk fibroin solution preparation, SEM, and nano-CT imaging.

All authors would like to acknowledge support from the University of Florida and the University of Florida Herbert Wertheim College of Engineering and Department of Chemical Engineering. Whitney L. Stoppel and Elizabeth L. Aikman acknowledge support from the William P and Tracy Cirioli Professorship at the University of Florida. Asha P. Rao and Emily E. Fussell recognize support from the University of Florida's Undergraduate University Scholars Program and the University of Florida Honors College. Elizabeth L. Aikman acknowledges support from the National Science Foundation Graduate Research Fellowship (DGE-2236414). Kayleigh E. Trumbull acknowledges support from the National Science Foundation Research Experience for Undergraduates (EEC-1852111). Any opinions, findings, and conclusions or recommendations expressed in this manuscript are those of the authors and do not necessarily reflect the views of the National Science Foundation.

CONFLICT OF INTEREST STATEMENT

The authors do not have any conflicts to report.

DATA AVAILABILITY STATEMENT

The data that supports the findings of this study are available and linked in the main manuscript, with an embedded link to the data's location: https://www.dropbox.com/sh/npy2vyh6p9yd764/AAC7TyZ3VYZuQ1xA72VrRLU2a?dl=0.

ORCID

Whitney L. Stoppel https://orcid.org/0000-0001-7467-1737

REFERENCES

1. Stoppel WL, Hu D, Domian IJ, Kaplan DL, Black LD 3rd. Anisotropic silk biomaterials containing cardiac extracellular matrix for cardiac tissue engineering. *Biomed Mater*. 2015;10(3):034105. doi:10.1088/1748-6041/10/3/034105
2. Kukla DA, Stoppel WL, Kaplan DL, Khetani SR. Assessing the compatibility of primary human hepatocyte culture within porous silk sponges. *RSC Adv*. 2020;10(62):37662-37674. doi:10.1039/d0ra04954a
3. Joukhdar H, Och Z, Tran H, et al. Imparting multi-scalar architectural control into silk materials using a simple multi-functional ice-Templating fabrication platform. *Adv Mater Technol*. 2023;8(8):2201642. doi:10.1002/admt.202201642
4. Rnjak-Kovacina J, DesRochers TM, Burke KA, Kaplan DL. The effect of sterilization on silk fibroin biomaterial properties. *Macromol Biosci*. 2015;15(6):861-874. doi:10.1002/mabi.201500013
5. Rnjak-Kovacina J, Wray LS, Burke KA, et al. Lyophilized silk sponges: a versatile biomaterial platform for soft tissue engineering. *ACS Biomater Sci Eng*. 2015;1(4):260-270. doi:10.1021/ab500149p
6. Rnjak-Kovacina J, Wray LS, Golinski JM, Kaplan DL. Arrayed hollow channels in silk-based scaffolds provide functional outcomes for engineering critically-sized tissue constructs. *Adv Funct Mater*. 2014;24(15):2188-2196. doi:10.1002/adfm.201302901
7. Jameson JF, Pacheco MO, Bender EC, et al. Impact of bioactive molecule inclusion in lyophilized silk scaffolds varies between in vivo and in vitro assessments. *bioRxiv*. 2022. doi:10.1101/2022.05.24.493207
8. Jameson JF, Pacheco MO, Butler JE, Stoppel WL. Estimating kinetic rate parameters for enzymatic degradation of lyophilized silk fibroin sponges. *Front bioeng biotechnol*. 2021;9(537):664306. doi:10.3389/fbioe.2021.664306
9. Stoppel WL, Ghezzi CE, McNamara SL, Black LD 3rd, Kaplan DL. Clinical applications of naturally derived biopolymer-based scaffolds for regenerative medicine. *Ann Biomed Eng*. 2015;43(3):657-680. doi:10.1007/s10439-014-1206-2
10. Abbott RD, Kimmerling EP, Cairns DM, Kaplan DL. Silk as a biomaterial to support long-term three-dimensional tissue cultures. *ACS Appl Mater Interfaces*. 2016;8(34):21861-21868. doi:10.1021/acsami.5b12114
11. Abbott RD, Wang RY, Reagan MR, et al. The use of silk as a scaffold for mature, sustainable unilocular adipose 3D tissue engineered systems. *Adv Healthc Mater*. 2016;5(13):1667-1677. doi:10.1002/adhm.201600211
12. Alave Reyes-Furrer A, De Andrade S, Bachmann D, et al. Matrigel 3D bioprinting of contractile human skeletal muscle models recapitulating exercise and pharmacological responses. *Commun Biol*. 2021;4(1):1183. doi:10.1038/s42003-021-02691-0
13. Volpi M, Paradiso A, Costantini M, Swieszkowski W. Hydrogel-based fiber biofabrication techniques for skeletal muscle tissue engineering. *ACS Biomater Sci Eng*. 2022;8(2):379-405. doi:10.1021/acsbiomaterials.1c01145
14. Barton ER, Pacak CA, Stoppel WL, Kang PB. The ties that bind: functional clusters in limb-girdle muscular dystrophy. *Skelet Muscle*. 2020;10(1):22. doi:10.1186/s13395-020-00240-7
15. Stoppel WL, Kaplan DL, Black LD 3rd. Electrical and mechanical stimulation of cardiac cells and tissue constructs. *Adv Drug Deliv Rev*. 2016;96:135-155. doi:10.1016/j.addr.2015.07.009
16. Lin X, Fan L, Wang L, Filppula AM, Yu Y, Zhang H. Fabricating biomimetic materials with ice-templating for biomedical applications. *Smart Med*. 2023;2(3):e20230017. doi:10.1002/SMMD.20230017
17. Diaz F, Forsyth N, Boccaccini AR. Aligned ice templated biomaterial strategies for the musculoskeletal system. *Adv Healthc Mater*. 2023;12(21):e2203205. doi:10.1002/adhm.202203205
18. Joukhdar H, Seifert A, Jüngst T, Groll J, Lord MS, Rnjak-Kovacina J. Ice templating soft matter: fundamental principles and fabrication approaches to tailor pore structure and morphology and their biomedical applications. *Adv Mater*. 2021;33(34):2100091. doi:10.1002/adma.202100091
19. Byette F, Bouchard F, Pellerin C, Paquin J, Marcotte I, Mateescu MA. Cell-culture compatible silk fibroin scaffolds concomitantly patterned by freezing conditions and salt concentration. *Polym Bull*. 2011;67(1):159-175. doi:10.1007/s00289-010-0438-z
20. Asuncion MCT, Goh JC-H, Toh S-L. Anisotropic silk fibroin/gelatin scaffolds from unidirectional freezing. *Mater Sci Eng C*. 2016;67:646-656. doi:10.1016/j.msec.2016.05.087
21. Mao M, He J, Liu Y, Li X, Li D. Ice-template-induced silk fibroin–chitosan scaffolds with predefined microfluidic channels and fully porous structures. *Acta Biomater*. 2012;8(6):2175-2184. doi:10.1016/j.actbio.2011.12.025
22. Mandal BB, Gil ES, Panilaitis B, Kaplan DL. Laminar silk scaffolds for aligned tissue fabrication. *Macromol Biosci*. 2012;13(1):48-58. doi:10.1002/mabi.201200230
23. Hu X, Shmelev K, Sun L, et al. Regulation of silk material structure by temperature-controlled water vapor annealing. *Biomacromolecules*. 2011;12(5):1686-1696. doi:10.1021/bm200062a
24. Hu X, Kaplan D, Cebe P. Dynamic protein-water relationships during β-sheet formation. *Macromolecules*. 2008;41(11):3939-3948. doi:10.1021/ma071551d
25. Zhou CZ, Confalonieri F, Jacquet M, Perasso R, Li ZG, Janin J. Silk fibroin: structural implications of a remarkable amino acid sequence. *Proteins*. 2001;44(2):119-122. doi:10.1002/prot.1078
26. Patel M, Dubey DK, Singh SP. Phenomenological models of *Bombyx mori* silk fibroin and their mechanical behavior using molecular dynamics simulations. *Mater Sci Eng C Mater Biol Appl*. 2020;108:110414.
27. Zhang L, Zhang W, Hu Y, et al. Systematic review of silk scaffolds in musculoskeletal tissue engineering applications in the recent decade. *ACS Biomater Sci Eng*. 2021;7(3):817-840. doi:10.1021/acsbiomaterials.0c01716
28. Rockwood DN, Preda RC, Yucel T, Wang X, Lovett ML, Kaplan DL. Materials fabrication from *Bombyx mori* silk fibroin. *Nat Protoc*. 2011;6(10):1612-1631. doi:10.1038/nprot.2011.379
29. Hu X, Kaplan D, Cebe P. Determining beta-sheet crystallinity in fibrous proteins by thermal analysis and infrared spectroscopy. *Macromolecules*. 2006;39(18):6161-6170. doi:10.1021/ma0610109

30. Fossey SA, Nemethy G, Gibson KD, Scheraga HA. Conformational energy studies of beta-sheets of model silk fibroin peptides. I. Sheets of poly(ala-Gly) chains. *Biopolymers*. 1991;31(13):1529-1541. doi:10.1002/bip.360311309
31. Humphrey W, Dalke A, Schulten K. VMD: visual molecular dynamics. *J Mol Graph*. 1996;14(1):33-38. doi:10.1016/0263-7855(96)00018-5
32. Abraham MJ, Murtola T, Schulz R, et al. GROMACS: high performance molecular simulations through multi-level parallelism from laptops to supercomputers. *SoftwareX*. 2015;1-2:19-25. doi:10.1016/j.softx.2015.06.001
33. Thompson AP, Aktulga HM, Berger R, et al. LAMMPS-a flexible simulation tool for particle-based materials modeling at the atomic, meso, and continuum scales. *Comput Phys Commun*. 2022;271:108171. doi:10.1016/j.cpc.2021.108171
34. Huang J, Rauscher S, Nawrocki G, et al. CHARMM36m: an improved force field for folded and intrinsically disordered proteins. *Nat Methods*. 2017;14(1):71-73. doi:10.1038/nmeth.4067
35. Shirts MR, Klein C, Swails JM, et al. Lessons learned from comparing molecular dynamics engines on the SAMPL5 dataset. *J Comput Aided Mol des*. 2017;31(1):147-161. doi:10.1007/s10822-016-9977-1
36. Ryckaert J-P, Ciccotti G, Berendsen HJC. Numerical integration of the cartesian equations of motion of a system with constraints: molecular dynamics of n-alkanes. *J Comput Phys*. 1977;23(3):327-341. doi:10.1016/0021-9991(77)90098-5
37. Pacheco MO, Lutz HM, Armada J, et al. Silk fibroin particles as carriers in the development of hemoglobin-based oxygen carriers. *Adv. NanoBiomed Res*. 2023;3:2300019. doi:10.1002/anbr.202300019
38. Callister J, William D, Rethwisch DG. *Fundamentals of Materials Science and Engineering: An Integrated Approach*. 5th ed. John Wiley and Sons, Inc; 2015:216-278.
39. Cheng L, Shao JX, Wang F, Li Z, Dai FY. Strain rate dependent mechanical behavior of B. mori silk, A. assama silk, A. pernyi silk and A. ventricosus spider silk. Materials & Design. 2020;195:108988. doi:10.1016/j.matdes.2020.108988
40. Morrow DA, Haut Donahue TL, Odegard GM, Kaufman KR. Transversely isotropic tensile material properties of skeletal muscle tissue. *J Mech Behav Biomed Mater*. 2010;3(1):124-129. doi:10.1016/j.jmbbm.2009.03.004
41. Kuthe CD, Uddanwadiker RV. Investigation of effect of fiber orientation on mechanical behavior of skeletal muscle. *J Appl Biomater Funct Mater*. 2016;14(2):154-162. doi:10.5301/jabfm.5000275
42. Brown J, Lu CL, Coburn J, Kaplan DL. Impact of silk biomaterial structure on proteolysis. *Acta Biomater*. 2015;11:212-221. doi:10.1016/j.actbio.2014.09.013
43. Asakura T, Okushita K, Williamson MP. Analysis of the structure of silk fibroin by NMR. *Macromolecules*. 2015;48(8):2345-2357. doi:10.1021/acs.macromol.5b00160
44. Huang WW, Krishnaji S, Tokareva OR, Kaplan D, Cebe P. Influence of water on protein transitions: morphology and secondary structure. *Macromolecules*. 2014;47(22):8107-8114. doi:10.1021/ma5016227
45. Inoue S, Tanaka K, Arisaka F, Kimura S, Ohtomo K, Mizuno S. Silk fibroin of *Bombyx mori* is secreted, assembling a high molecular mass elementary unit consisting of H-chain, L-chain, and P25, with a 6:6:1 molar ratio. *J Biol Chem*. 2000;275(51):40517-40528. doi:10.1074/jbc.M006897200
46. Hossain D, Tschopp MA, Ward DK, Bouvard JL, Wang P, Horstemeyer MF. Molecular dynamics simulations of deformation mechanisms of amorphous polyethylene. *Polymer*. 2010;51(25):6071-6083. doi:10.1016/j.polymer.2010.10.009
47. Mezger TG. Oscillatory Tests. Applied Rheology: With Joe Flow on Rheology Road. 5th ed. Graz, Austria: Anton Paar GmbH. 2018. 89–100.
48. Jalal S, Dastidar S, Tedesco FS. Advanced models of human skeletal muscle differentiation, development and disease: three-dimensional cultures, organoids and beyond. *Curr Opin Cell Biol*. 2021;73:92-104. doi:10.1016/j.ceb.2021.06.004
49. Jiang Y, Torun T, Maffioletti SM, Serio A, Tedesco FS. Bioengineering human skeletal muscle models: recent advances, current challenges and future perspectives. *Exp Cell Res*. 2022;416(2):113133. doi:10.1016/j.yexcr.2022.113133
50. Ostrovidov S, Ramalingam M, Bae H, et al. Latest developments in engineered skeletal muscle tissues for drug discovery and development. *Expert Opin Drug Discovery*. 2023;18(1):47-63. doi:10.1080/17460441.2023.2160438
51. Mihaly E, Altamirano DE, Tuffaha S, Grayson W. Engineering skeletal muscle: building complexity to achieve functionality. *Semin Cell Dev Biol*. 2021;119:61-69. doi:10.1016/j.semcdb.2021.04.016
52. Vesga-Castro C, Aldazabal J, Vallejo-Illarramendi A, Paredes J. Contractile force assessment methods for in vitro skeletal muscle tissues. *Elife*. 2022;11:e77204. doi:10.7554/eLife.77204
53. Somers SM, Spector AA, DiGirolamo DJ, Grayson WL. Biophysical stimulation for engineering functional skeletal muscle. *Tissue Eng Part B Rev*. 2017;23(4):362-372. doi:10.1089/ten.TEB.2016.0444
54. Somers SM, Zhang NY, Morrissette-McAlmon JBF, Tran K, Mao HQ, Grayson WL. Myoblast maturity on aligned microfiber bundles at the onset of strain application impacts myogenic outcomes. *Acta Biomater*. 2019;94:232-242. doi:10.1016/j.actbio.2019.06.024
55. Somers SM, Grayson WL. Protocol for the use of a novel bioreactor system for hydrated mechanical testing, strained sterile culture, and force of contraction measurement of tissue engineered muscle constructs. *Front Cell Dev Biol*. 2021;9:661036. doi:10.3389/fcell.2021.661036
56. Qazi TH, Wu J, Muir VG, et al. Anisotropic rod-shaped particles influence injectable granular hydrogel properties and cell invasion. *Adv Mater*. 2022;34(12):e2109194. doi:10.1002/adma.202109194
57. McCuller C, Jessu R, Callahan AL. Physiology, Skeletal Muscle. StatPearls. Treasure Island (FL): StatPearls Publishing Copyright © 2023, StatPearls Publishing LLC. 2023.
58. Carnes ME, Pins GD. Skeletal muscle tissue engineering: biomaterials-based strategies for the treatment of volumetric muscle loss. *Bioengineering (Basel)*. 2020;7(3):85. doi:10.3390/bioengineering7030085

SUPPORTING INFORMATION

Additional supporting information can be found online in the Supporting Information section at the end of this article.

How to cite this article: Aikman EL, Rao AP, Jia Y, et al. Impact of crystalline domains on long-term stability and mechanical performance of anisotropic silk fibroin sponges. *J Biomed Mater Res*. 2024;1-21. doi:10.1002/jbm.a.37703